# CHAPTER IV

# EXPERIMENTAL RESULTS

# Chapter IV

# EXPERIMENTAL RESULTS

## 4.1 INTRODUCTION

In this chapter, the parameters of the system and the plasma are determined using different diagnostic techniques.

The total discharge current and the discharge voltage drop are measured by means of Rogowsky coil and capacitive potential divider, respectively. The knowledge of the total current and voltage drop leads to the calculation of the total inductance and resistance of the system, plasma inductance and resistance and their variation with discharge time.

By using the double electric probe, the electron temperature and plasma density are obtained. The plasma sheath velocity variation is measured by magnetic probes inserted inside the plasma and by using of pick up loops wounded around the outer electrode.

## 4.2 ELECTRICAL PARAMETERS

This section is devoted to study the variation of the discharge current, voltage and power with discharge time.

### *4.2.1 Discharge Current Variation*

Figure ( 4 – 1 ) represents the variation of the discharge current with time at 3 kV charging voltage and 0.19 Torr pressure. It appears from the figure that the discharge current signal follow the relation [6, 23]

$$I = I_o \sin\omega t \exp\left(-\frac{R_t\, t}{2\, L_t}\right) \qquad (4\text{-}1)$$

Where $I$ is the discharge current, $I_o$ is the peak discharge current, $R_t$ is the total circuit resistance and $L_t$ is the total circuit inductance.

This equation means that the sinusoidal current $I_o \sin \omega t$ decreases by a factor equal to $\exp(-R_t t / 2L_t)$.

The value of the discharge current $I$ can be obtained from equation ( 3 - 5 ) as

$$I = \frac{V_o RC}{Ab\mu_o}$$

Where $b$ is the winding density ( $N/2\pi r$ ) and r is the major radius then, the discharge current is calculated from the equation ( 3 - 6 ) as

$$I = 3260\ V_o$$

Hence for $3\ kV$ charging voltage of the capacitor bank, the peak current at the first and second half cycles are $8.809\ kA$ and $7.667\ kA$, respectively.

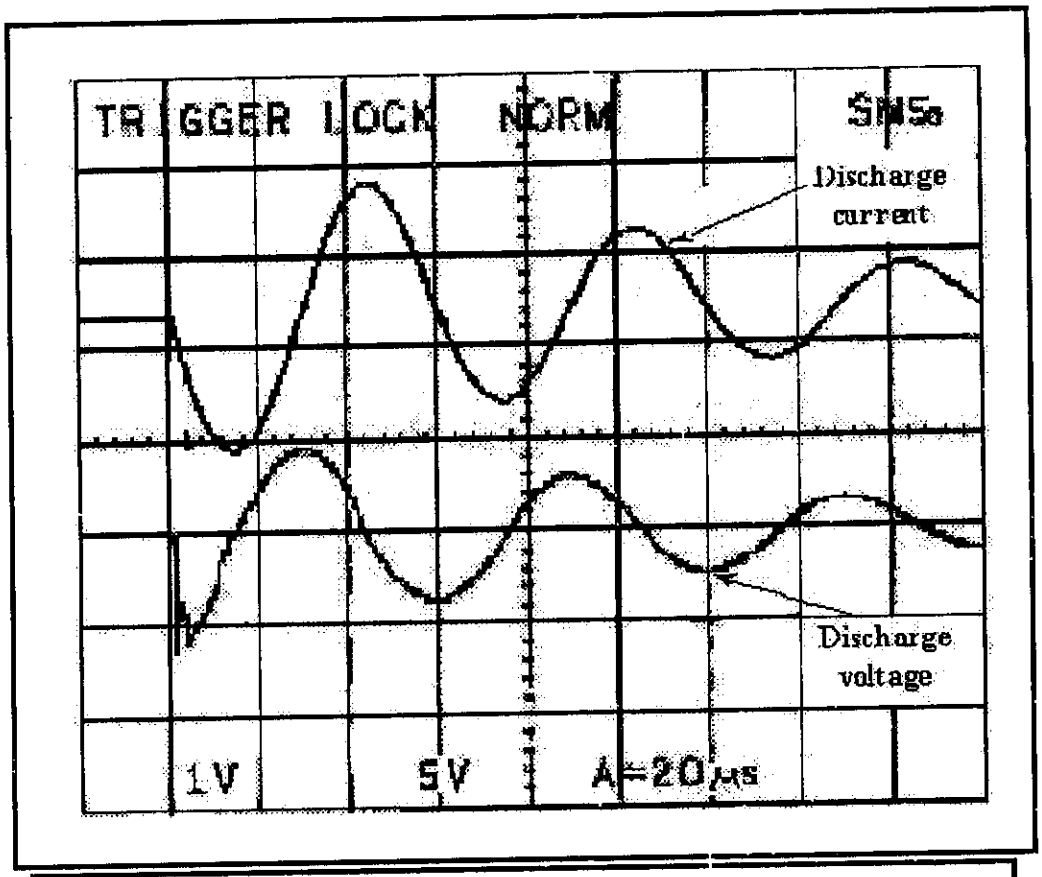


Fig. ( 4 – 1 ) Current and voltage signals at 3 kV charging voltage and 0.19 Torr pressure.

### 4.2.2 *Potential Across the Coaxial Accelerator*

A capacitive coupling potential divider is used to measure the variation of the potential as a function of discharge time. Figure ( 4 – 1 ) shows the potential variation between the coaxial electrodes at 3 kV charging voltage and 0.19 Torr pressure. It is clear that the voltage variation looks like the current variation behavior but with a phase shift.

A calibration of the potential divider using known voltage is made to be able to measure the potential drop $V$ according to the signals recorded on the oscilloscope $V_{out}$ which is given in equation ( 3 - 10 ) as

$$V_{in} = 333.3\ V_{out}$$

### 4.2.3 *Discharge Power Variation*

Figure ( 4 – 2 ) shows the variation of the discharge power with time at the same conditions of Fig. ( 4 - 1 ). The power is obtained by multiplying the two signals of the discharge current and voltage. The positive value of the power signal flows by the capacitor induced electric field and the negative part is the power flows by the generated magnetic field from the discharge circuit inductance. The power signal showed the flow of it from the capacitor bank in the positive direction and from the inductance of the circuit in the opposite direction. The peak power achieved for *3 kV* charging voltage was *10.37 MW.*

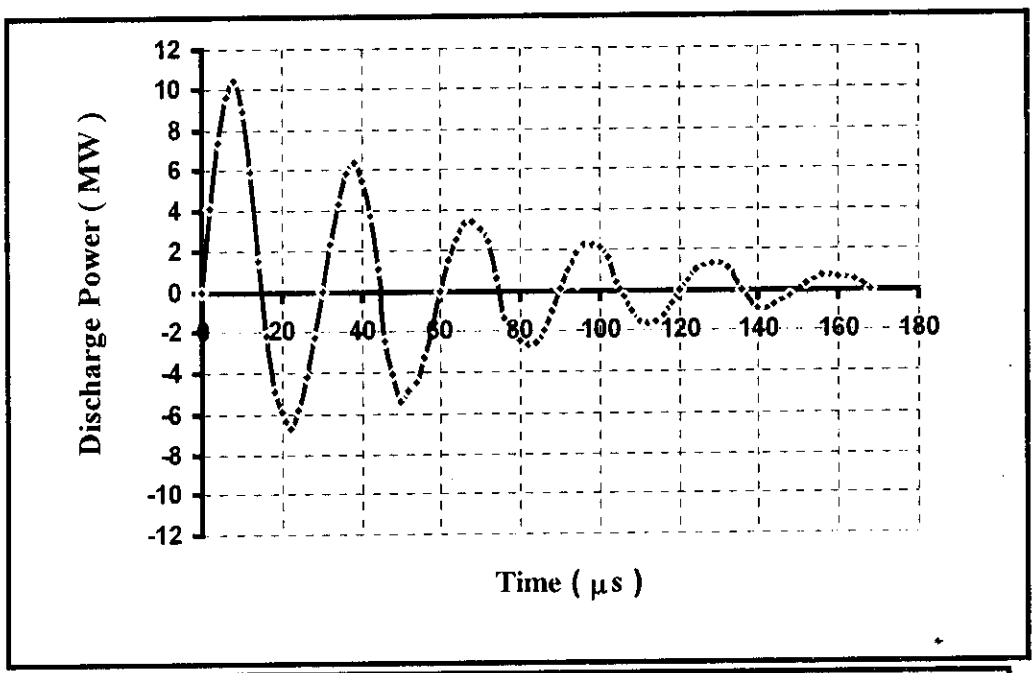


Fig. ( 4 – 2 ) The power signal at 3 kV charging voltage and 0.19 Torr pressure.

## 4.3 ELECTRICAL CIRCUIT ANALYSIS

Figure ( 4 – 3 ) shows the equivalent circuit of the plasma coaxial discharge system. In this circuit it is assumed that the total circuit resistance $R_t$ consists of two parts, plasma sheath resistance $R_p$ and the resistance of the material components of the circuit $R_c$ such as the cables, switch and the capacitors rather than the plasma itself. This can be expressed mathematically by the equation

$$R_t = R_p + R_c \qquad (4-2)$$

The same idea is applied to the total circuit inductance $L_t$ to be equal to the plasma inductance itself $L_p$ including the portion of the coaxial electrodes and the circuit components inductance $L_c$

$$L_t = L_p + L_c \qquad (4-3)$$

The condenser bank $C$ is charged by the power supply and a voltage drop $V(t)$ appears through the plasma source itself due to the discharge current $I(t)$ passes through it.

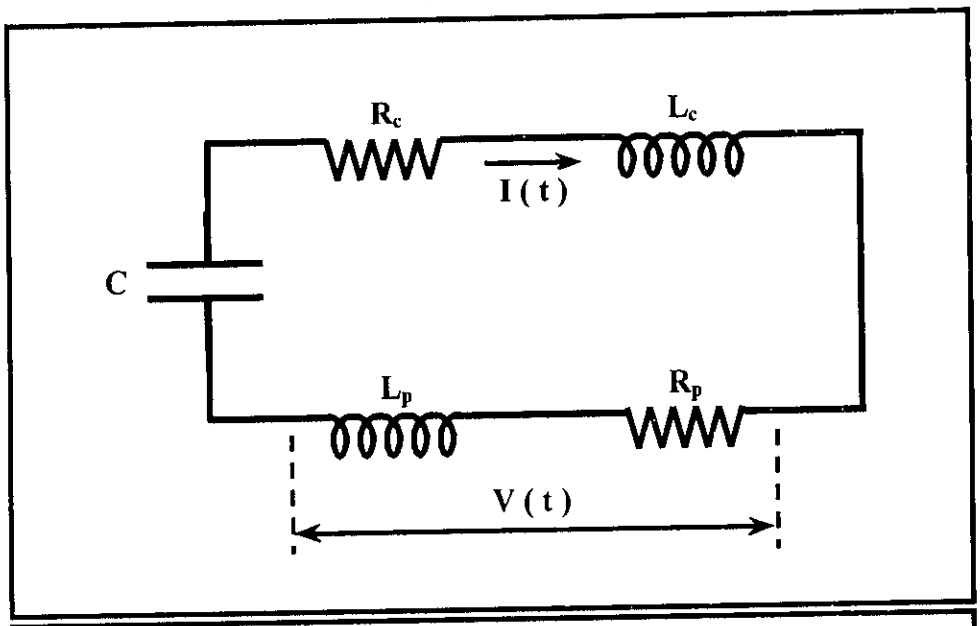


Fig. ( 4 – 3 ) Equivalent electrical circuit of the coaxial plasma discharge system.

### 4.3.1 Determination of Total Circuit Inductance

The total circuit inductance is determined from the resonance condition in the *R-L-C* circuit neglecting the total circuit resistance

$$\omega L_t = \frac{1}{\omega C} \qquad (4-4)$$

Where ω is the frequency = $2\pi/\tau$ ,then one gets

$$\tau = 2\pi\sqrt{L_t C} \qquad (4-5)$$

So the total circuit inductance is given by

$$L_t = \frac{\tau^2}{4\pi^2 C} \qquad (4-6)$$

The condenser bank $C$ has a capacity equals to $46.26\ \mu F$ so, for $3\ kV$ charging voltage where the periodic time τ is equal to $60\ \mu s$ as shown in Fig. ( 4 – 1 ) then, the total circuit inductance $L_t$ is equal to $1.97\ \mu H$.

### 4.3.2 Determination of Total Circuit Resistance

As mentioned previously, the discharge current passes through the circuit is given by equation ( 4 – 1 ) as

$$I = I_o \sin\omega t \ exp\left(-\frac{R_t\, t}{2\, L_t}\right)$$

For $\omega t = n\pi/2$ where $n = 1, 3, 5, \ldots \sin\omega t = 1$ then

$$I_p = I_o \ exp\left(-\frac{R_t\, t}{2\, L_t}\right) \qquad (4-7)$$

The last equation is satisfied only at the points of the peak current $I_p$ where the maximum value of the current appears at every half period only.

Taking the logarithm of equation ( 4 – 7 ) then

$$ln\, I_p = \left( -\frac{R_t\, t}{2\, L_t} \right) - ln\, I_o \qquad (4-8)$$

Plotting the relation between $ln\, I_p$ and the discharge time one get a straight line of negative slope equal to $-R_t / 2L_t$. Then the total circuit resistance $R_t$ can be determined by knowing the $L_t$ value.

As shown in Fig. ( 4 – 1 ), the maximum peak current $I_o$, which is the first peak, appears less than the expected value , and this is due to the energy losses in ionizing the gas between the two coaxial electrodes and in the spark gap switch. The expected value of $I_o$ can be obtained directly from the straight line relation between $ln\, I_p$ and the discharge time at the time corresponding to that peak.

The values of the peak current and the discharge time are listed in Table ( 4 – 1 ). The relation between $ln\, I_p$ and the discharge time is obtained at $3\ kV$ charging voltage and $0.19\ Torr$ pressure as shown in Fig. ( 4 - 4 ). The slope is equal to $-9.35 \times 10^3\ \Omega/H$. Then the total circuit resistance is equal to

$$R_T = -2L_T \times slope = -2 \times (1.97 \times 10^{-6}) \times (-9.35 \times 10^3) = 36.87\ m\Omega$$

| Time ( μs ) | 15 | 45 | 75 | 105 | 135 | 166 |
|---|---|---|---|---|---|---|
| $I_p$ ( kA ) | 8.809 | 7.667 | 5.873 | 4.731 | 3.426 | 2.447 |
| Ln $I_p$ | 9.084 | 8.945 | 8.678 | 8.462 | 8.139 | 7.803 |

Table ( 4 – 1 )

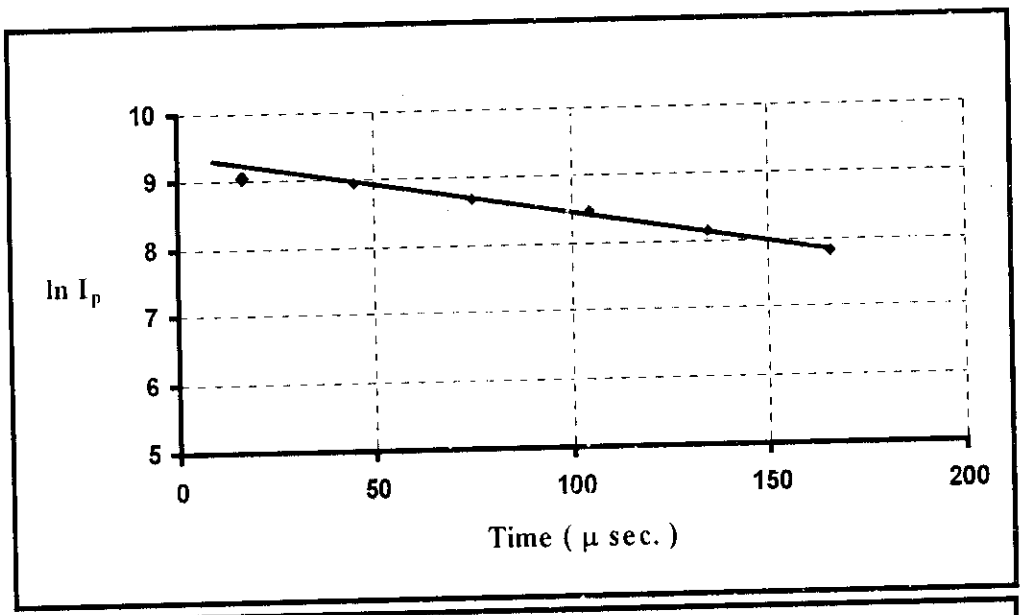


Fig. ( 4 – 4 ) Relation between ln $I_p$ and the discharge time at 3 kV charging voltage and 0.19 Torr pressure.

### 4.3.3 *Determination of Plasma Inductance*

The voltage drop across the plasma $V(t)$ consists of two parts, the first one, equal to that across the plasma inductance which is varying with time, and the other across the plasma resistance which is negligable compared to the voltage drop across the inductance ( it is clear from the trace of Fig. ( 4 – 1) ). Therefore, the voltage across the plasma itself can be established as [6, 23]

$$V(t) = I(t)\,R_p(t) + \frac{d}{dt}\left[L_p(t)\,I(t)\right] \qquad (4\text{-}9)$$

Neglecting the voltage drop across the plasma resistance compared to that across the plasma inductance ( $V_R < V_L$ ) so

$$V(t) = \frac{d}{dt}\left[L_p(t)\,I(t)\right] \qquad (4\text{-}10)$$

Consider that the plasma inductance $L_p(t)$ is constant in the interval $\Delta t$ then

$$L_p(t) = \frac{V(t)}{d\,I(t)/dt} \qquad (4\text{-}11)$$

By dividing the signal of the discharge current into parts each of width $\Delta t$ and plotting the relation between $V(t)/\{(I_2-I_1)/(t_2-t_1)\}$ and the discharge time, one gets the plasma inductance variation with time.

The data obtained from the voltage and current signals are recorded in Table ( 4 – 2 ). The plasma inductance is plotted as a function of the discharge time in Fig. ( 4 – 5 ) for *3 kV* charging voltage and *0.19 Torr* pressure.

| t ( μs ) | V ( kV ) | dI/dt $\times 10^6$ A/s | L ( μH ) |
|---|---|---|---|
| 4 | 1.933 | 863.541 | 2.239 |
| 8 | 1.533 | 602.190 | 2.546 |
| 12 | 0.700 | 248.054 | 2.822 |
| 16 | -0.250 | -135.234 | 1.848 |
| 20 | -0.800 | -481.427 | 1.662 |
| 24 | -1.167 | -733.021 | 1.591 |
| 28 | -1.333 | -850.714 | 1.567 |
| 32 | -1.367 | -820.807 | 1.665 |
| 36 | -1.233 | -651.040 | 1.894 |
| 40 | -0.800 | -376.812 | 2.123 |
| 44 | -0.133 | -48.598 | 2.743 |
| 48 | 0.567 | 275.806 | 2.054 |
| 52 | 0.900 | 541.378 | 1.662 |
| 56 | 1.100 | 705.122 | 1.560 |
| 60 | 1.200 | 699.362 | 1.716 |
| 64 | 1.000 | 575.701 | 1.737 |
| 68 | 0.750 | 401.465 | 1.868 |
| 72 | 0.417 | 165.372 | 2.519 |
| 76 | -0.233 | -90.157 | 2.588 |
| 80 | -0.500 | -320.955 | 1.558 |
| 84 | -0.767 | -488.687 | 1.569 |
| 88 | -0.933 | -567.150 | 1.645 |
| 92 | -0.933 | -506.485 | 1.843 |
| 96 | -0.750 | -401.729 | 1.867 |
| 100 | -0.500 | -232.515 | 2.150 |
| 104 | -0.067 | -29.988 | 2.223 |
| 108 | 0.250 | 170.188 | 1.469 |
| 112 | 0.500 | 334.061 | 1.497 |
| 116 | 0.667 | 435.101 | 1.532 |
| 120 | 0.800 | 420.678 | 1.902 |

Table ( 4 – 2 )

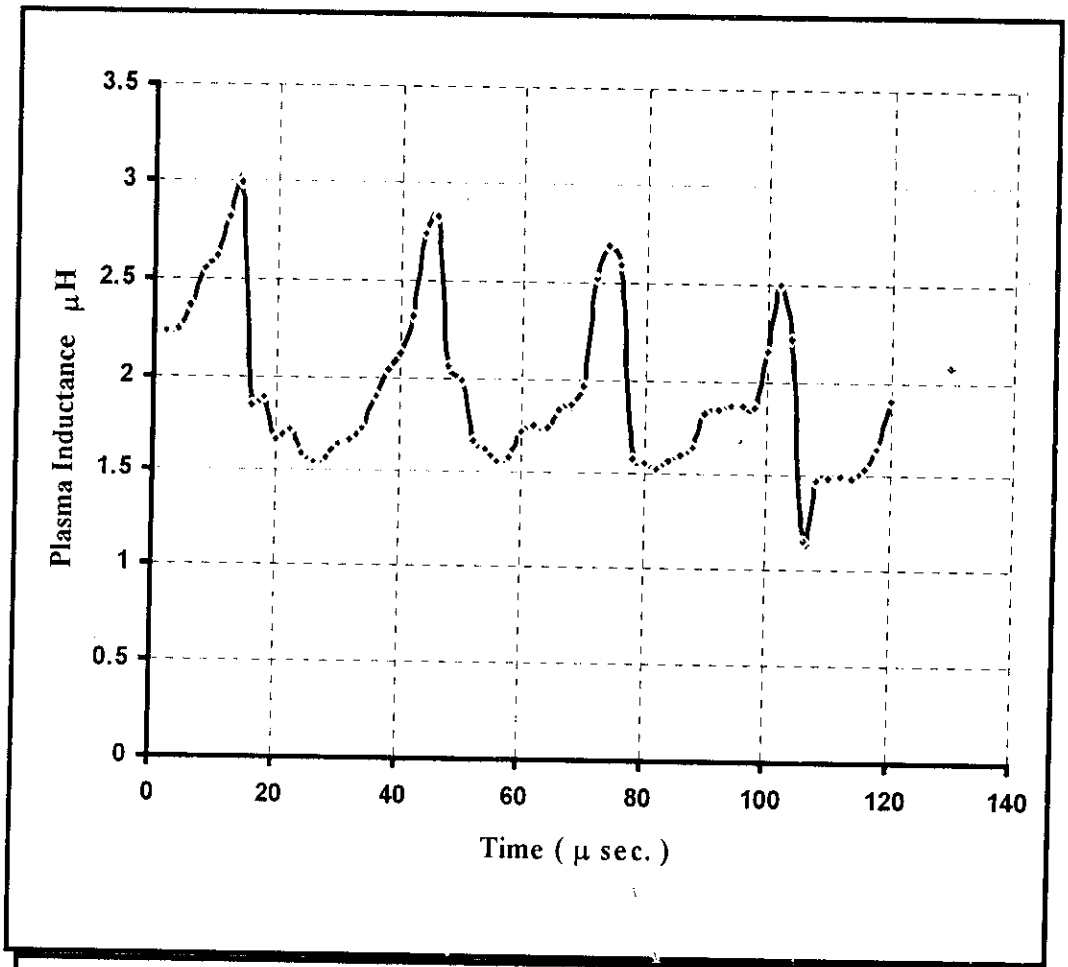


**Fig. ( 4 – 5 ) The plasma inductance versus discharge time relation at 3 kV charging voltage and 0.19 Torr pressure.**

| t ( μs ) | I ( kA ) | V ( kV ) | L ( μH ) | $L1I1 \times 10^{-3}$ ( H.A ) | $L2I2 \times 10^{-3}$ ( H.A ) | R ( mΩ ) |
|---|---|---|---|---|---|---|
| 4 | 3.772 | 1.933 | 2.239 | 4.334 | 12.754 | 45.560 |
| 8 | 6.764 | 1.533 | 2.546 | 12.754 | 20.441 | 57.445 |
| 12 | 8.496 | 0.700 | 2.822 | 20.441 | 26.269 | 89.109 |
| 16 | 8.719 | -0.250 | 1.848 | 26.269 | 15.639 | 276.103 |
| 20 | 7.452 | -0.800 | 1.662 | 15.639 | 10.862 | 52.910 |
| 24 | 4.964 | -1.167 | 1.591 | 10.862 | 5.250 | 47.661 |
| 28 | 1.723 | -1.333 | 1.567 | 5.250 | 0.000 | 12.045 |
| 32 | -1.694 | -1.367 | 1.665 | 0.000 | -5.678 | 31.322 |
| 36 | -4.700 | -1.233 | 1.894 | -5.678 | -11.981 | 72.835 |
| 40 | -6.797 | -0.800 | 2.123 | -11.981 | -17.124 | 71.487 |
| 44 | -7.660 | -0.133 | 2.743 | -17.124 | -21.490 | 125.093 |
| 48 | -7.190 | 0.567 | 2.054 | -21.490 | -12.898 | 219.970 |
| 52 | -5.514 | 0.900 | 1.662 | -12.898 | -6.997 | 104.347 |
| 56 | -2.962 | 1.100 | 1.560 | -6.997 | -2.363 | 19.774 |
| 60 | 0.000 | 1.200 | 1.716 | -2.363 | 2.270 | 0.000 |
| 64 | 2.515 | 1.000 | 1.737 | 2.270 | 6.618 | 34.580 |
| 68 | 4.510 | 0.750 | 1.868 | 6.618 | 10.220 | 33.439 |
| 72 | 5.664 | 0.417 | 2.519 | 10.220 | 15.761 | 171.006 |
| 76 | 5.813 | -0.233 | 2.588 | 15.761 | 8.688 | 264.048 |
| 80 | 4.968 | -0.500 | 1.558 | 8.688 | 6.449 | 12.032 |
| 84 | 3.309 | -0.767 | 1.569 | 6.449 | 3.640 | 19.393 |
| 88 | 1.149 | -0.933 | 1.645 | 3.640 | 0.000 | 20.263 |
| 92 | -1.045 | -0.933 | 1.843 | 0.000 | -3.786 | 12.584 |
| 96 | -2.900 | -0.750 | 1.867 | -3.786 | -6.739 | 3.980 |
| 100 | -4.194 | -0.500 | 2.150 | -6.739 | -11.416 | 159.571 |
| 104 | -4.727 | -0.067 | 2.223 | -11.416 | -5.373 | 333.724 |
| 108 | -4.436 | 0.250 | 1.469 | -5.373 | -5.933 | 87.926 |
| 112 | -3.402 | 0.500 | 1.497 | -5.933 | -3.950 | 1.222 |
| 116 | -1.828 | 0.667 | 1.532 | -3.950 | -1.519 | 32.237 |

Table ( 4 – 3 )

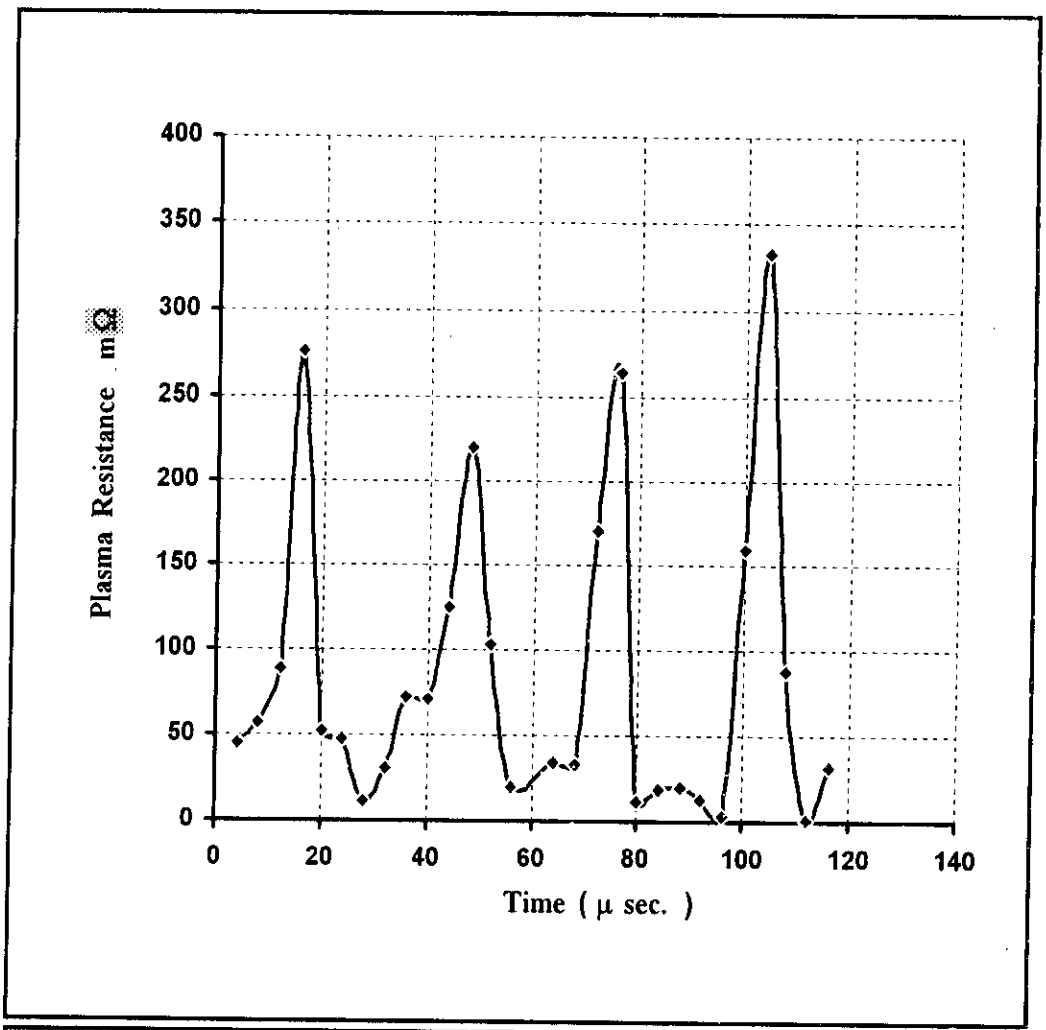


**Fig. ( 4 – 6 ) The plasma resistance versus the discharge time relation at 3 kV charging voltage and 0.19 Torr pressure.**

## 4.4 DOUBLE ELECTRIC PROBE MEASUREMENTS

The *I-V* characteristics curves for the double electric probe has been obtained to determine the electron temperature and plasma density.

### *4.4.1 Determination of Electron Temperature*

Figures ( 4 – 7 ) to ( 4 – 13 ) show the double electric probe signals at different potential differences for *3 kV* charging voltage and *0.19 Torr* pressure. As shown in these figures there are a peak in the probe signal occurs near the current peak.

By plotting the relation between the probe current $i_d$ and the probe voltage $V_d$ at certain time, one gets the double electric probe characteristic curve and the electron temperature is obtained from equation ( 3 – 19 ) . Another easy method to estimate the electron temperature is to determine the potential difference $V_{sd}$ between the two saturation probe current then, the plasma electron temperature is equal to ¼ $V_{sd}$.[22, 24] And for the identical probes as in the present work, the electron temperature is equal to ½ $V_{sd}$ of each branch of the characteristic curve.

Most of the electric probe characteristic curves can not easily determine the position of the saturation current. Since the probe current $I_d$ is an exponential relation, hence by drawing $ln\ I_d$ versus probe potential, one can get accurately the position of the saturation of the saturation current.

Figures from ( 4 – 14 ) to ( 4 – 19 ) show the relation between $I_d$ versus $V_d$ and $ln\ I_d$ versus $V_d$.

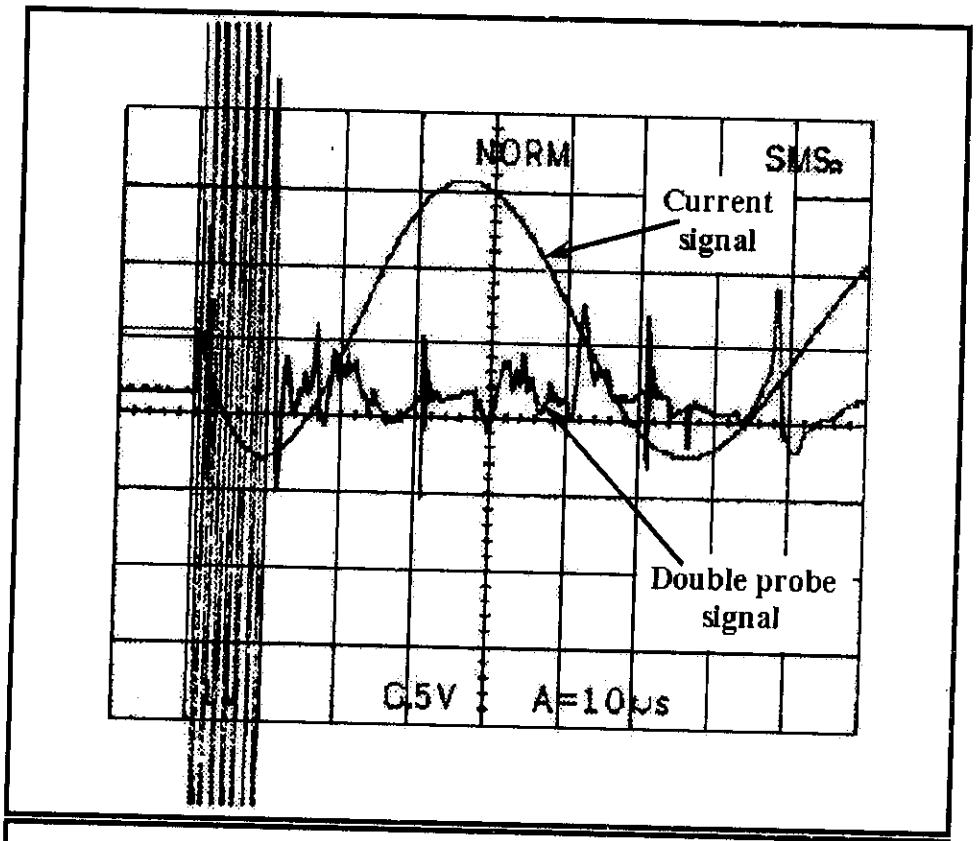


Fig. ( 4 – 7 ) Double electric probe signal at 3 kV charging voltage, 0.19 Torr pressure and zero volt for the probe potential.

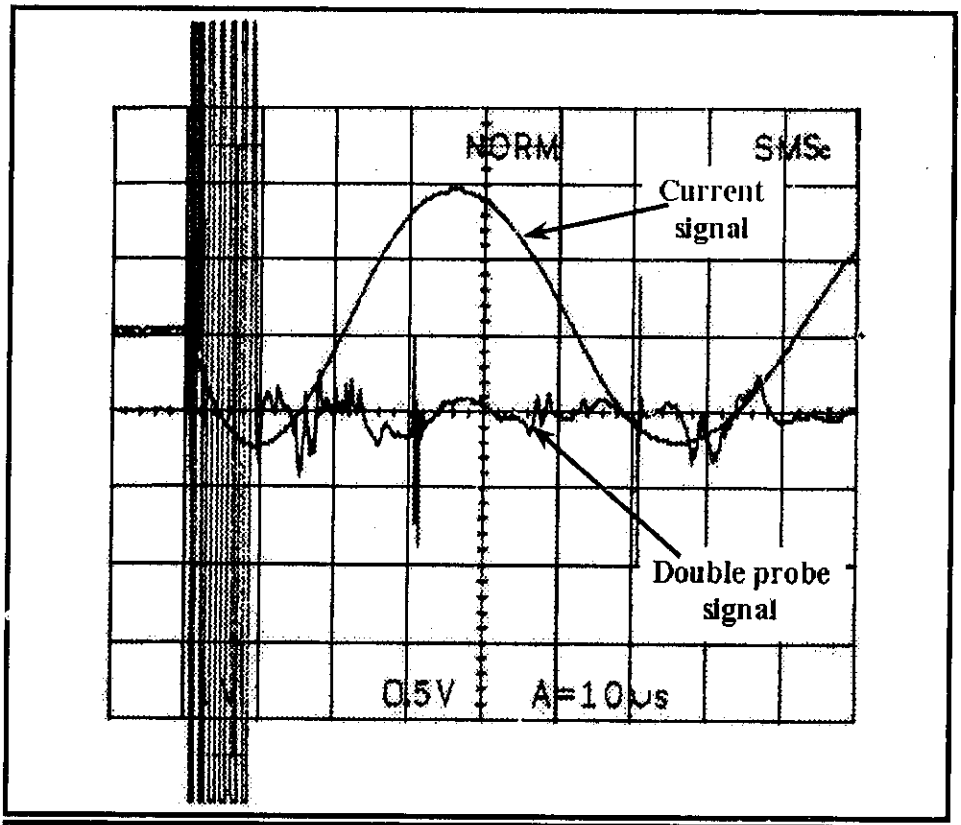


Fig. ( 4 – 8 ) Double electric probe signal at 3 kV charging voltage, 0.19 Torr pressure and 1.57 volt for the probe potential.

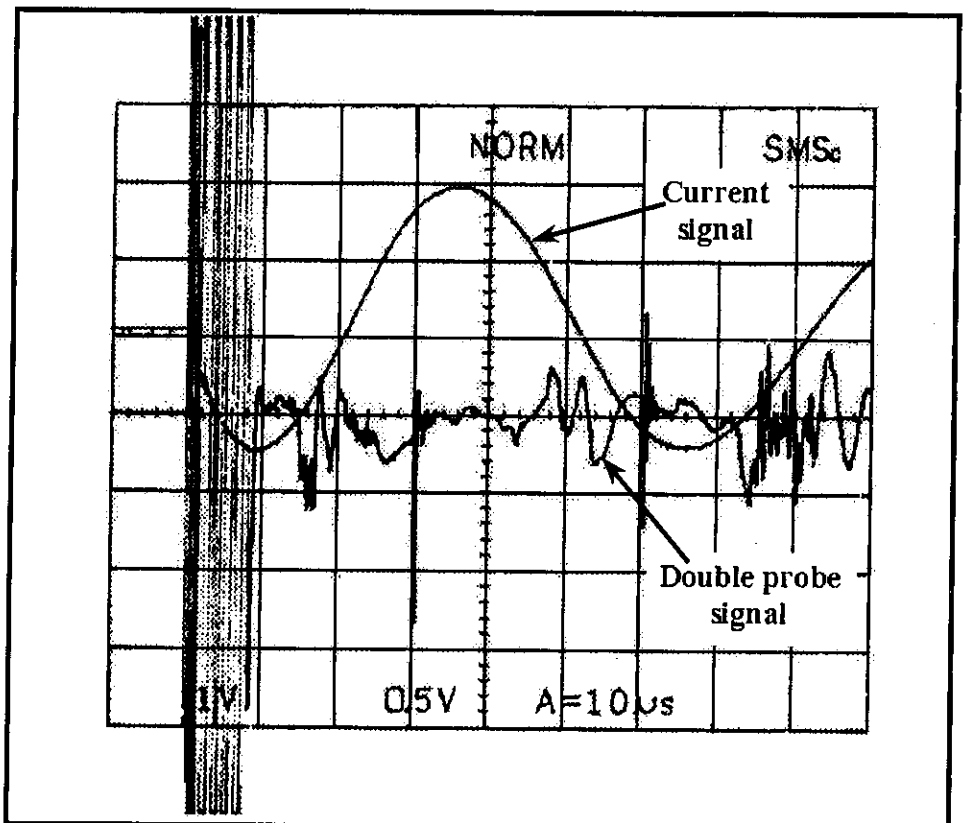


Fig. ( 4 – 9 ) Double electric probe signal at 3 kV charging voltage, 0.19 Torr pressure and 3.16 volt for the probe potential.

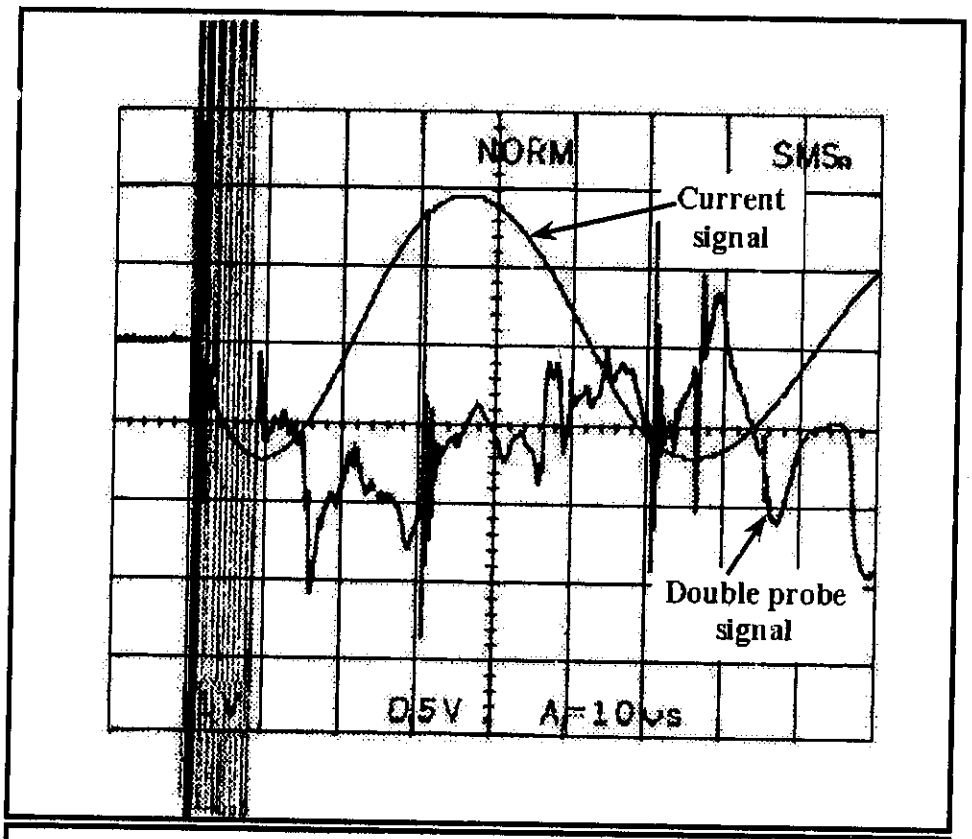


Fig. ( 4 - 10 ) Double electric probe signal at 3 kV charging voltage, 0.19 Torr pressure and 4.75 volt for the probe potential.

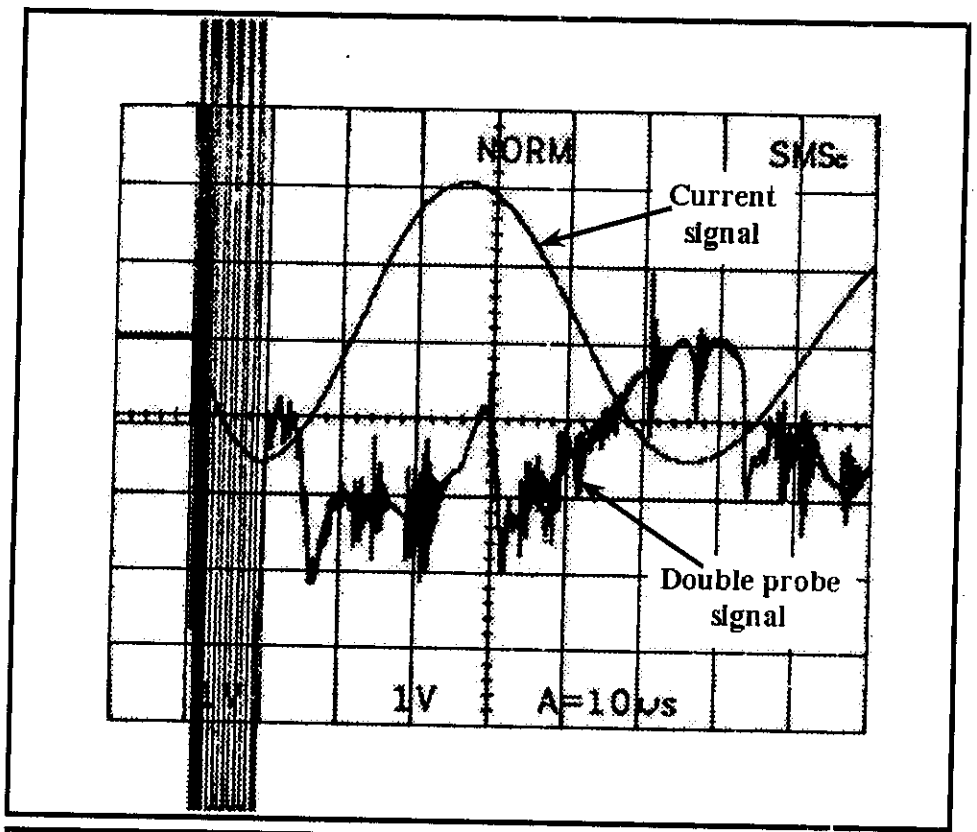


Fig. ( 4 - 11 ) Double electric probe signal at 3 kV charging voltage, 0.19 Torr pressure and 6.44 volt for the probe potential.

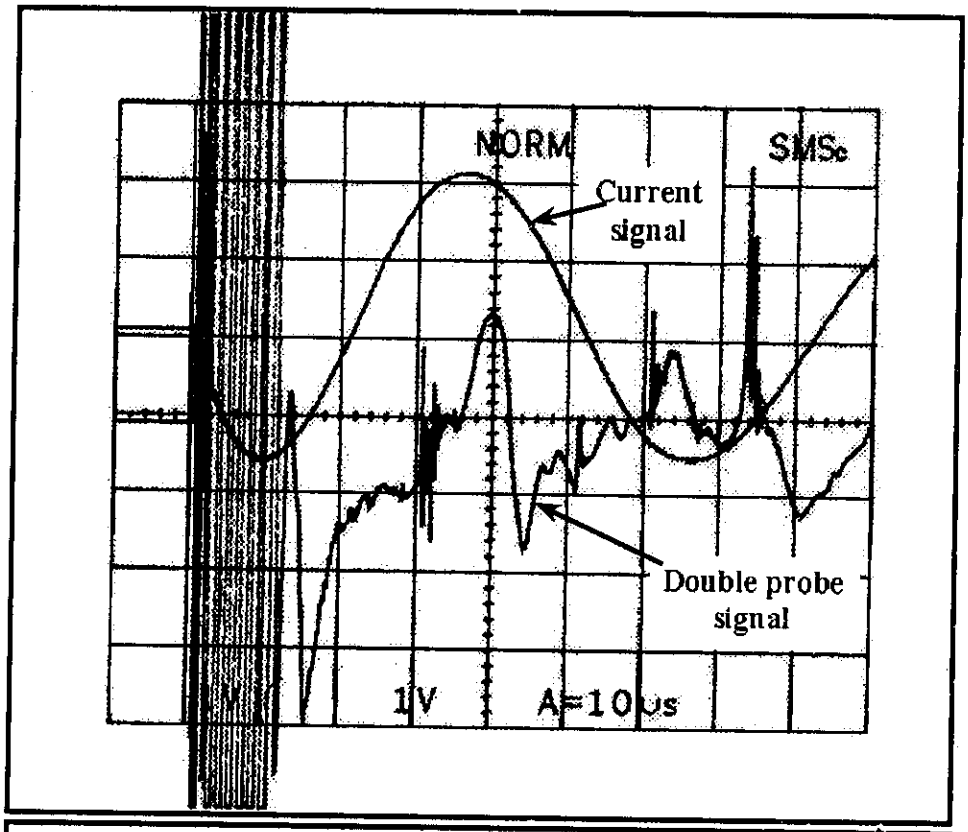


Fig. ( 4 - 12 ) Double electric probe signal at 3 kV charging voltage, 0.19 Torr pressure and 11.4 volt for the probe potential.

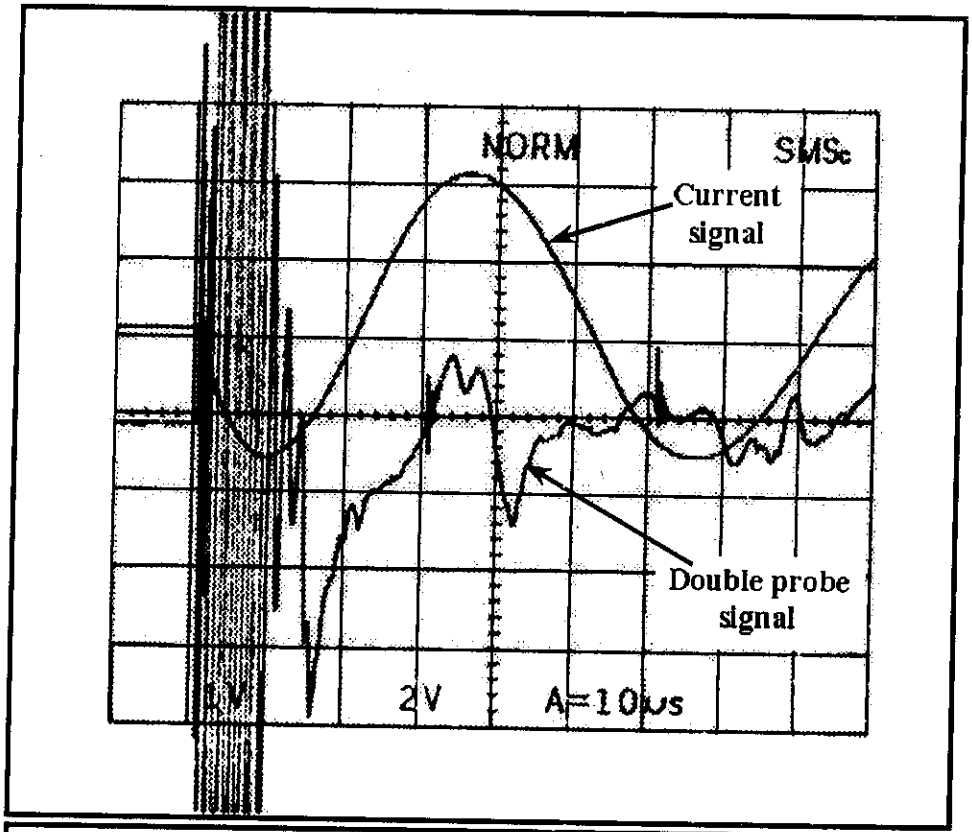


Fig. ( 4 - 13 ) Double electric probe signal at 3 kV charging voltage, 0.19 Torr pressure and 21.3 volt for the probe potential.

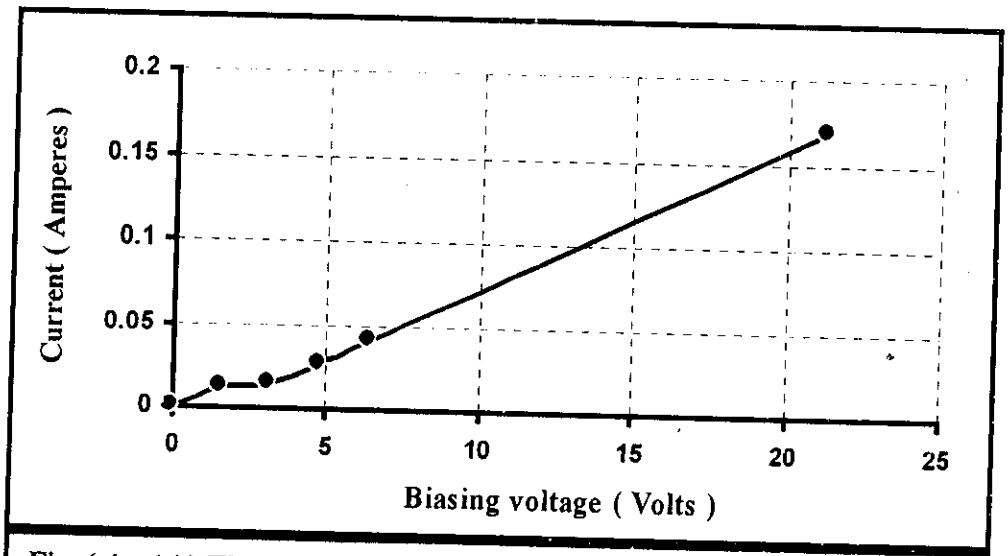


Fig. ( 4 – 14 ) The electric probe current versus voltage relation at 3 kV charging voltage and 0.19 Torr pressure for the 1st probe peak.

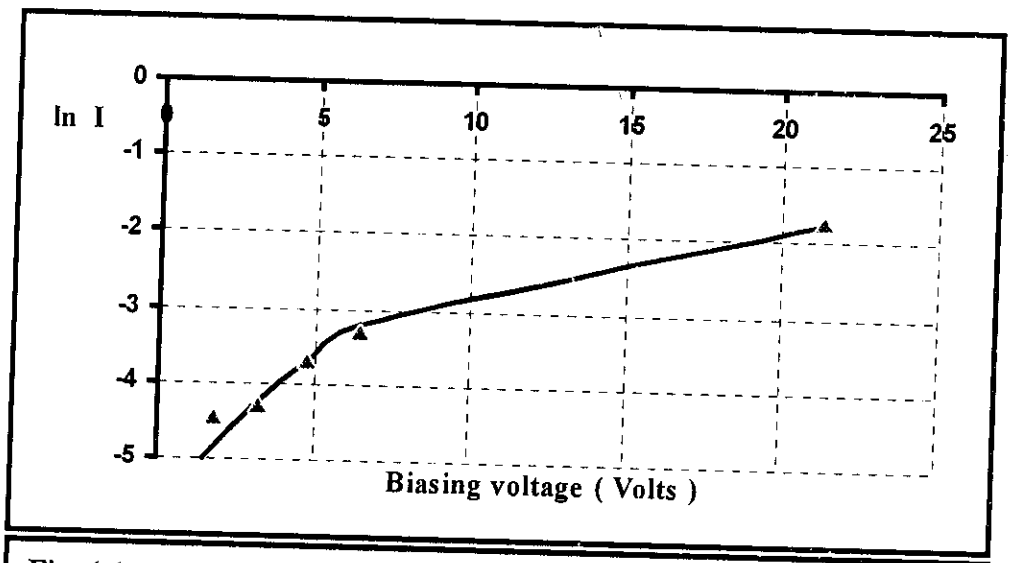


Fig. ( 4 – 15 ) The relation between ln I and probe voltage at 3 kV charging voltage and 0.19 Torr pressure for the 1st probe peak.

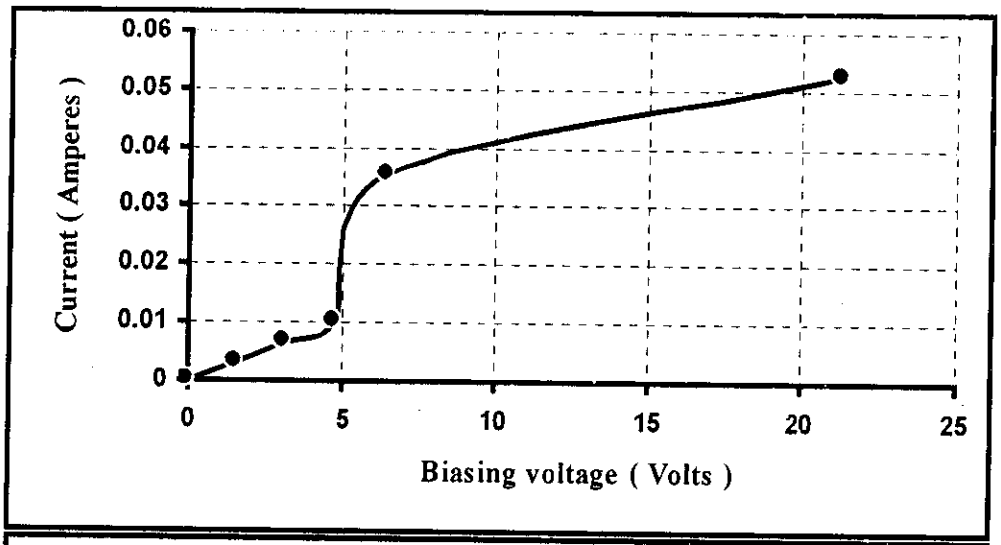


Fig. ( 4 – 16 ) The electric probe current versus voltage relation at 3 kV charging voltage and 0.19 Torr pressure for the 2nd probe peak.

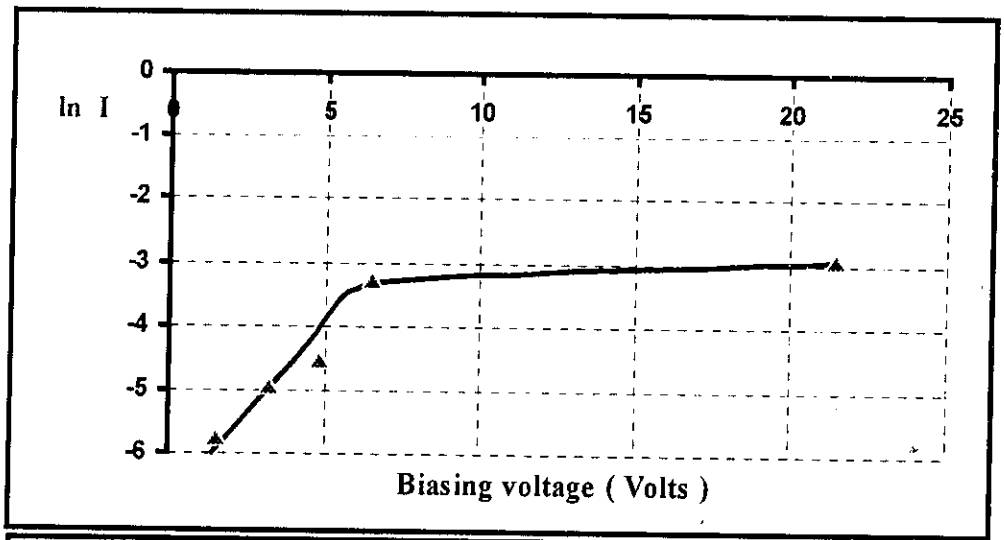


Fig. ( 4 – 17 ) The relation between ln I and probe voltage at 3 kV charging voltage and 0.19 Torr pressure for the 2nd probe peak.

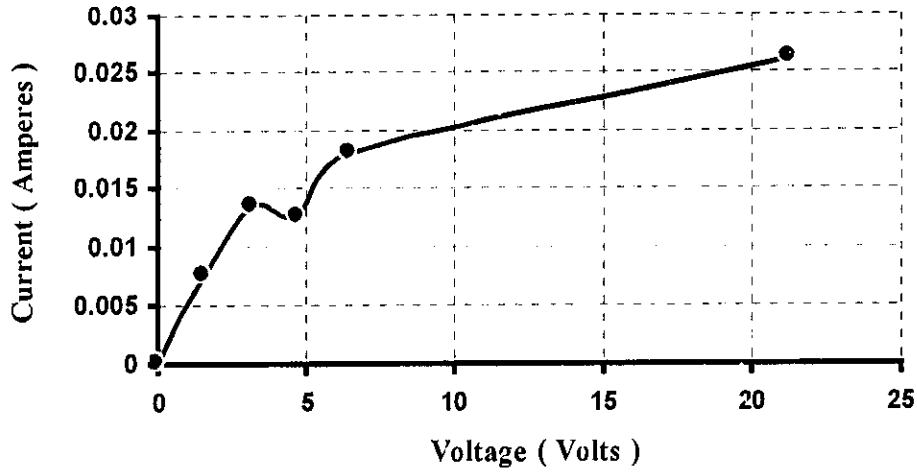


Fig. ( 4 – 18 ) The electric probe current versus voltage relation at 3 kV charging voltage and 0.19 Torr pressure for the 3rd probe peak.

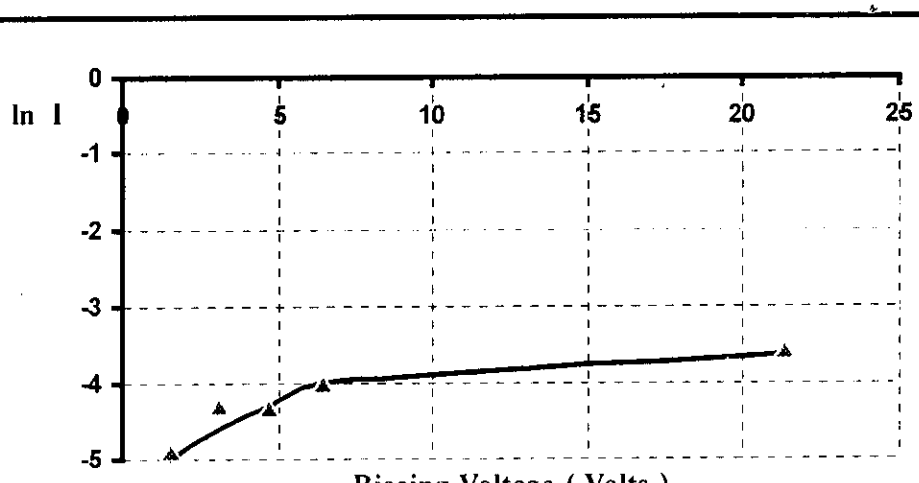


Fig. ( 4 – 19 ) The relation between ln I and probe voltage at 3 kV charging voltage and 0.19 Torr pressure for the 3rd probe peak.

### 4.4.2 *Determination of Plasma Ion Density*

The plasma ion density can be calculated from the relation (3 - 21)

$$I = \frac{1}{4} n_i e A_p (2kT_e / m_i)^{1/2}$$

Table ( 4 – 4 ) shows a summary for the electron temperature and ion density for the first three peaks of the double electric probe signals.

| Peak No | Saturation current ( mA ) | Electron Temperature ( eV ) | Ion density $\times 10^{13}$ ( $cm^{-3}$ ) |
|---|---|---|---|
| $1^{st}$ | 39 | 3.05 | 2.692 |
| $2^{nd}$ | 33.5 | 2.95 | 2.351 |
| $3^{rd}$ | 17 | 2.8 | 1.225 |

Table ( 4 – 4 )

## 4.5 SHEATH DYNAMICS MEASUREMENTS

In the present work two techniques are used to measure the plasma velocity, namely; pick up loops and magnetic probe.

### *4.5.1 Pick-up Loops*

The pick-up loops are wounded around the outer electrode of the system and almost at the breach. The space between the two loops is *1.8 cm.* This system is characterized by its measurement of the axial magnetic field attached with the plasma sheath. Due to the short length of electrode, the axial magnetic field is very small. This means that the pickup coils are not suitable for measuring the plasma velocity in the present work. [23]

### *4.5.2 Magnetic Probe Measurements*

The plasma sheath velocity in the $z$ direction is measured by two magnetic probes. The two probes are separated by *2 cm.* The velocity can be measured directly from equation ( 3 – 11 )

$$\text{sheath velocity}(v) = \frac{\text{distance between the two coils}(d)}{\text{phase difference}\ (\eta)}$$

Figures from ( 4 – 20 ) to ( 4 – 24 ) show the magnetic probe signals at various distances above the inner electrode for constant charging voltage and pressure equal to *3 kV* and *1 Torr* , respectively. The relation between the measured plasma sheath velocity and the probe position is shown in Table ( 4 – 5 ), and Fig. ( 4 – 27 ) shows this relation for the first and the second signal peaks.

Figure ( 4 – 27 ) shows that the axial sheath velocity decreases with position outside the accelerator up to certain distance then increased after. This can be due to the transfer of part of the axial velocity to radial one due to the electromagnetic lens at the muzzle. [25]

Figures ( 4 – 23 ), ( 4 – 25 ) and ( 4 – 26 ) show the magnetic probe signals at 1.7 cm above the inner electrode and 1 Torr pressure for various charging voltage. The relation between the plasma velocity and the charging voltage is shown in Table ( 4 – 6 ) and in Fig. ( 4 – 28 ).

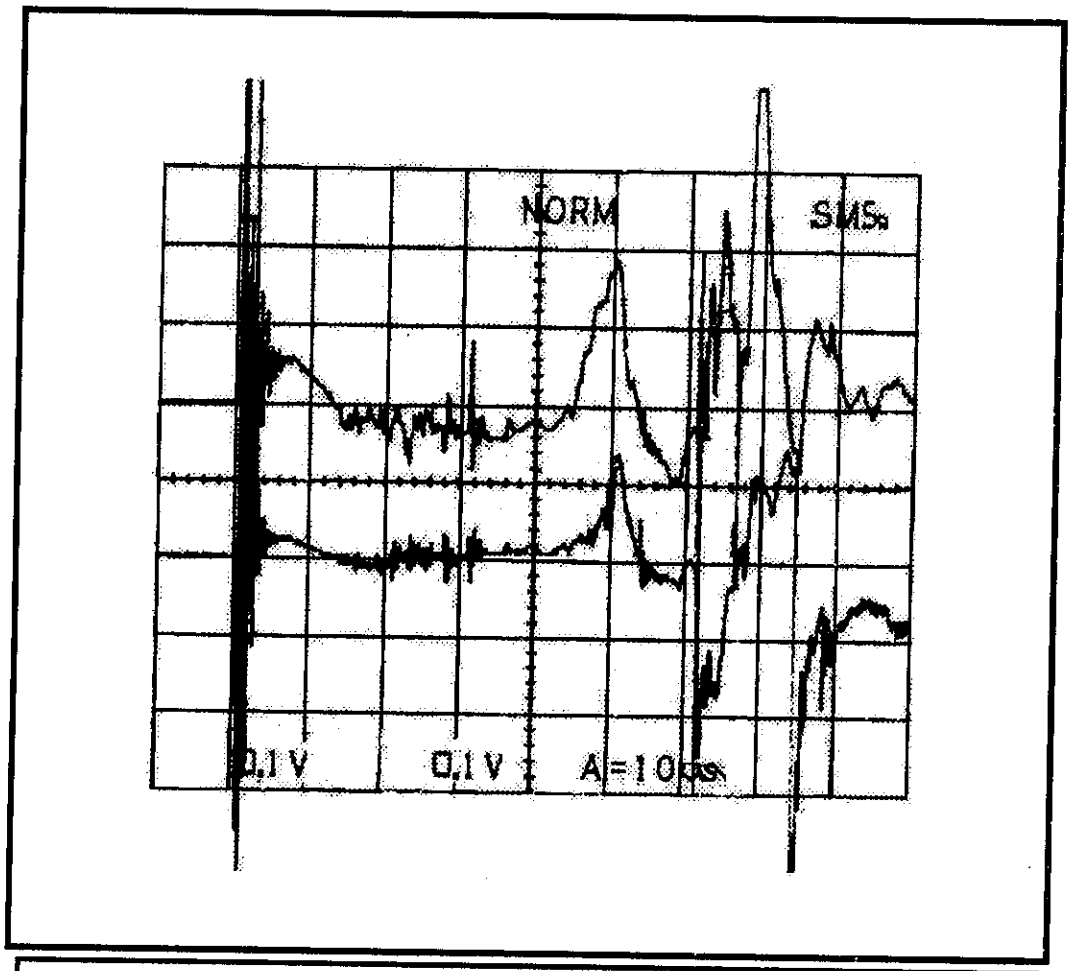


Fig. ( 4 - 20 ) Magnetic probes signals at 3 kV charging voltage, 1 Torr pressure and at a distance 4.7 cm above the inner electrode.

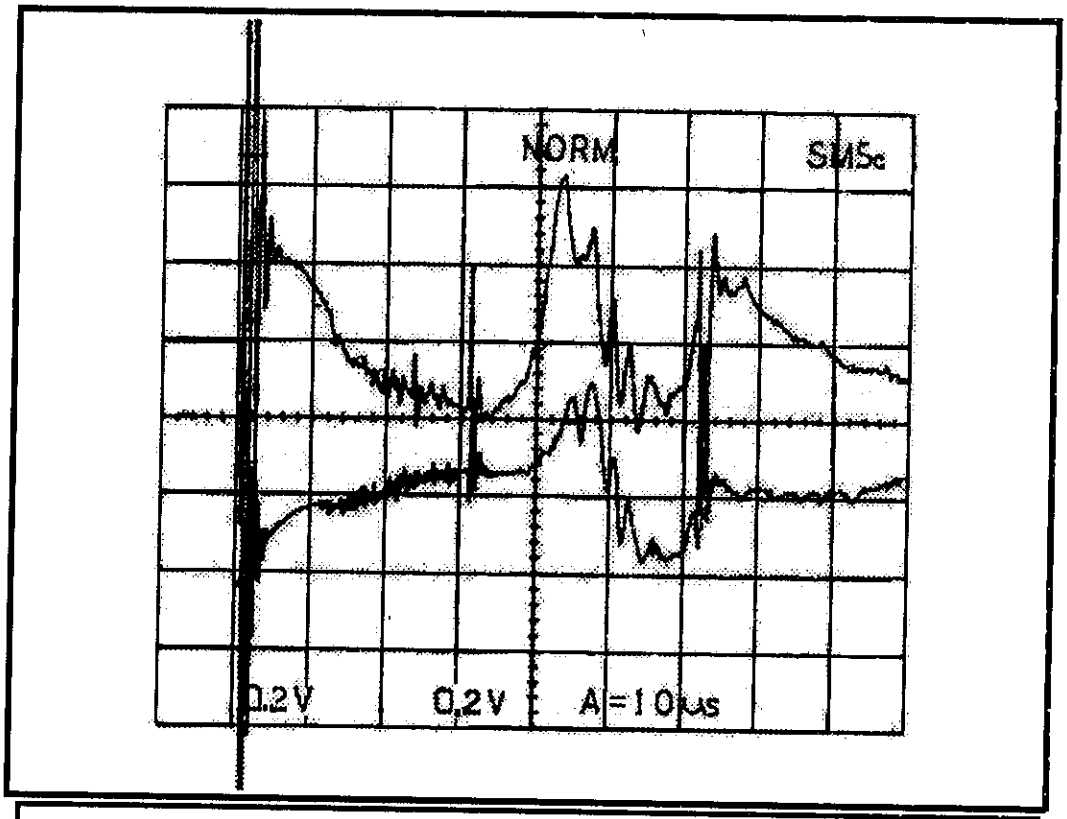


Fig. ( 4 - 21 ) Magnetic probes signals at 3 kV charging voltage, 1 Torr pressure and at a distance 3.7 cm above the inner electrode.

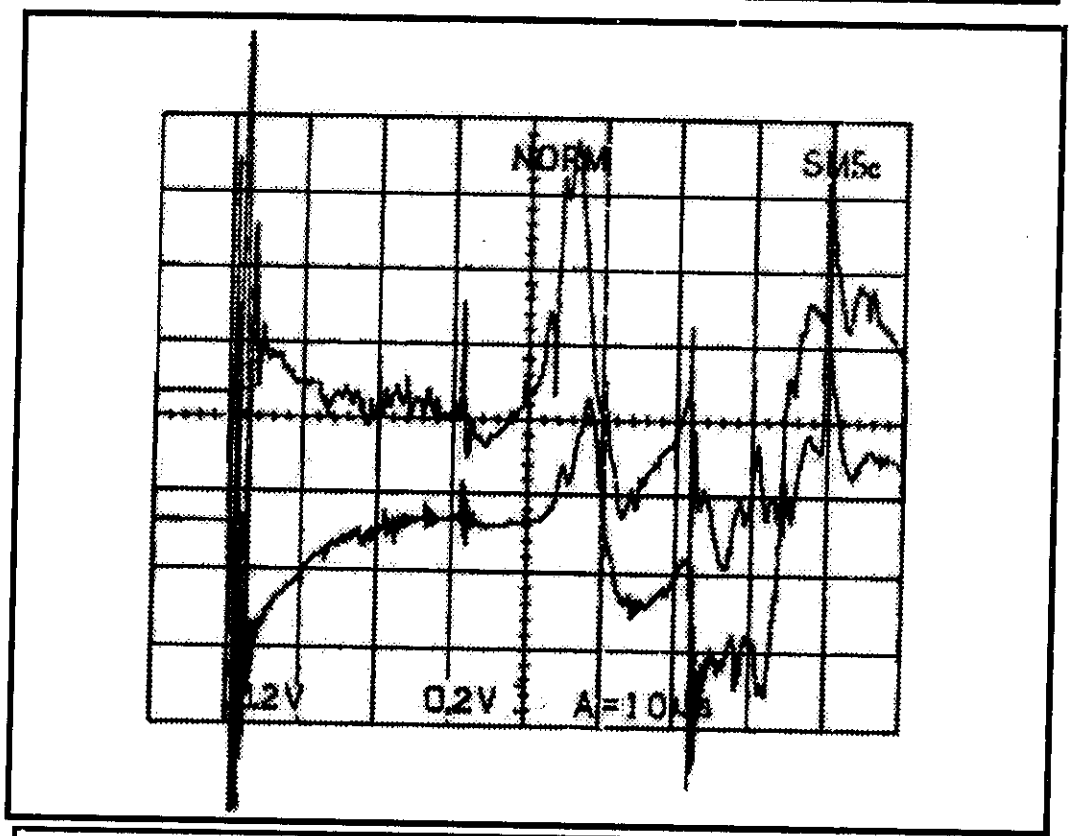


Fig. ( 4 - 22 ) Magnetic probes signals at 3 kV charging voltage, 1 Torr pressure and at a distance 2.7 cm above the inner electrode.

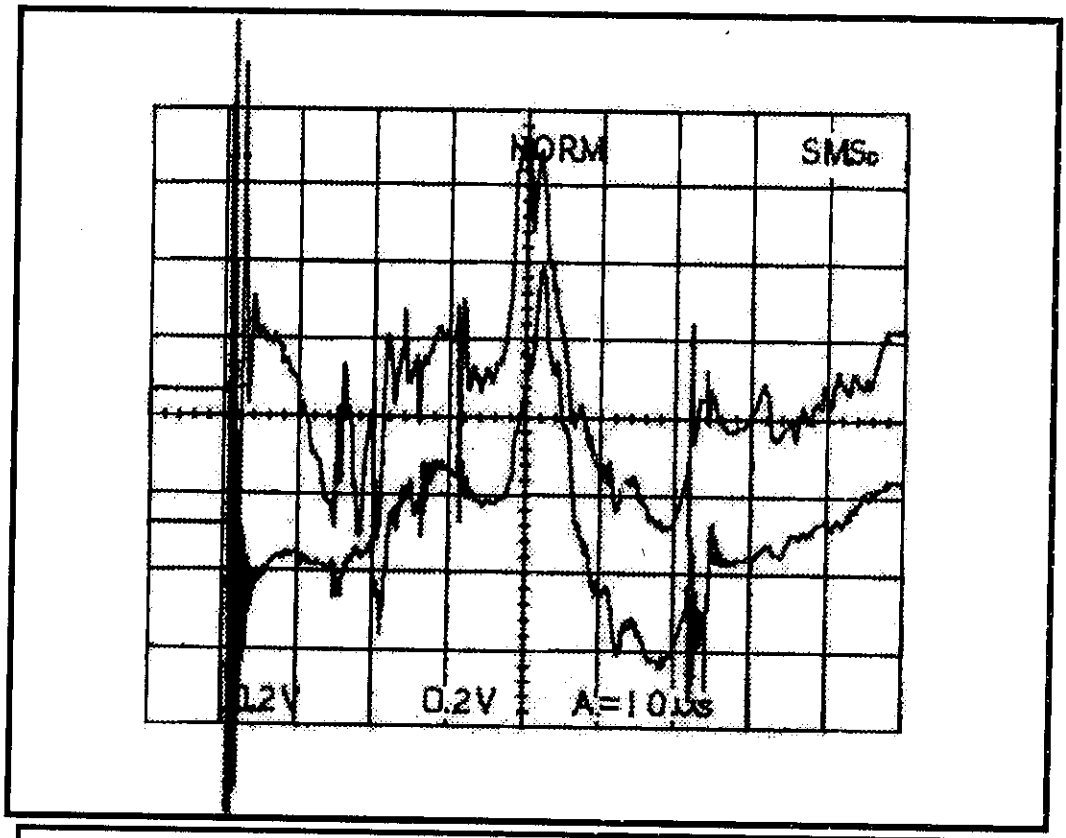


Fig. ( 4 - 23 ) Magnetic probes signals at 3 kV charging voltage, 1 Torr pressure and at a distance 1.7 cm above the inner electrode.

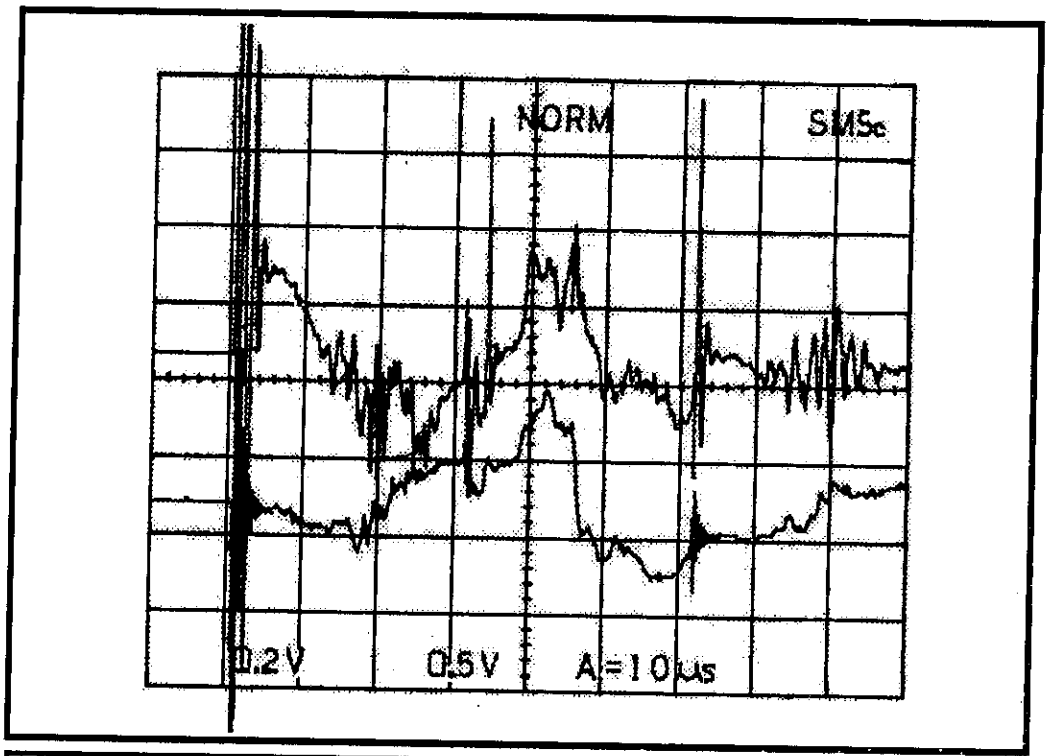


Fig. ( 4 - 24 ) Magnetic probes signals at 3 kV charging voltage, 1 Torr pressure and at a distance 0.7 cm above the inner electrode.

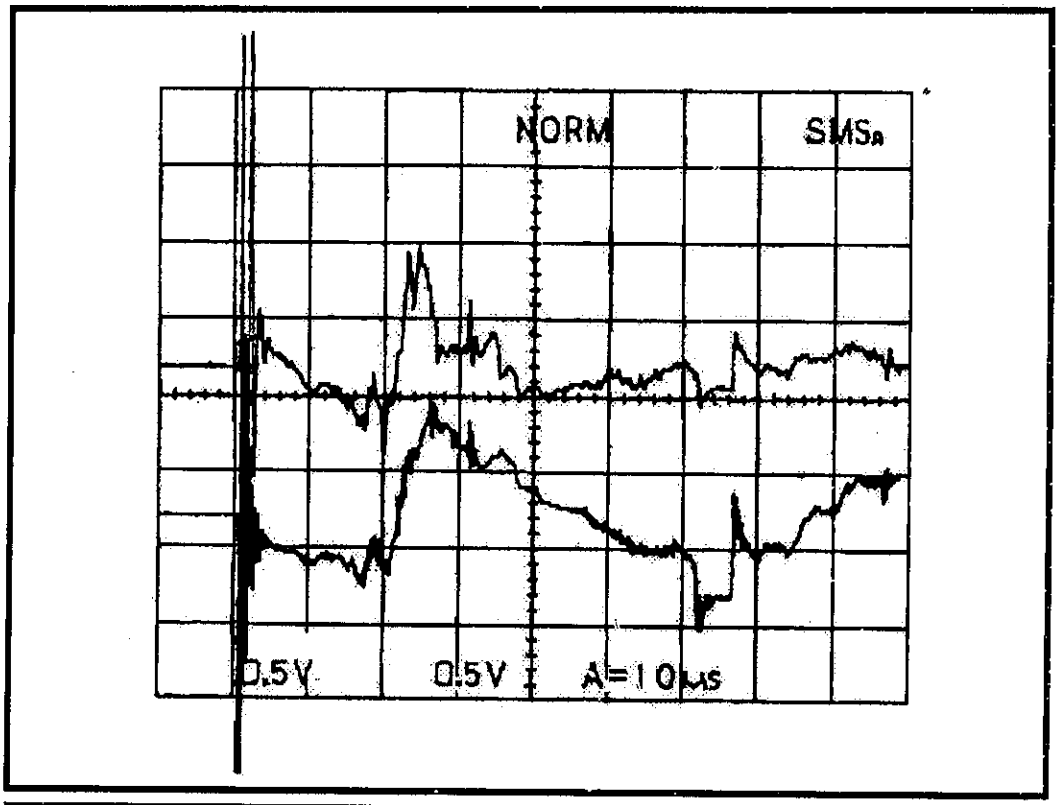


Fig. ( 4 - 25 ) Magnetic probes signals at 4.5 kV charging voltage, 1 Torr pressure and at a distance 1.7 cm above the inner electrode.

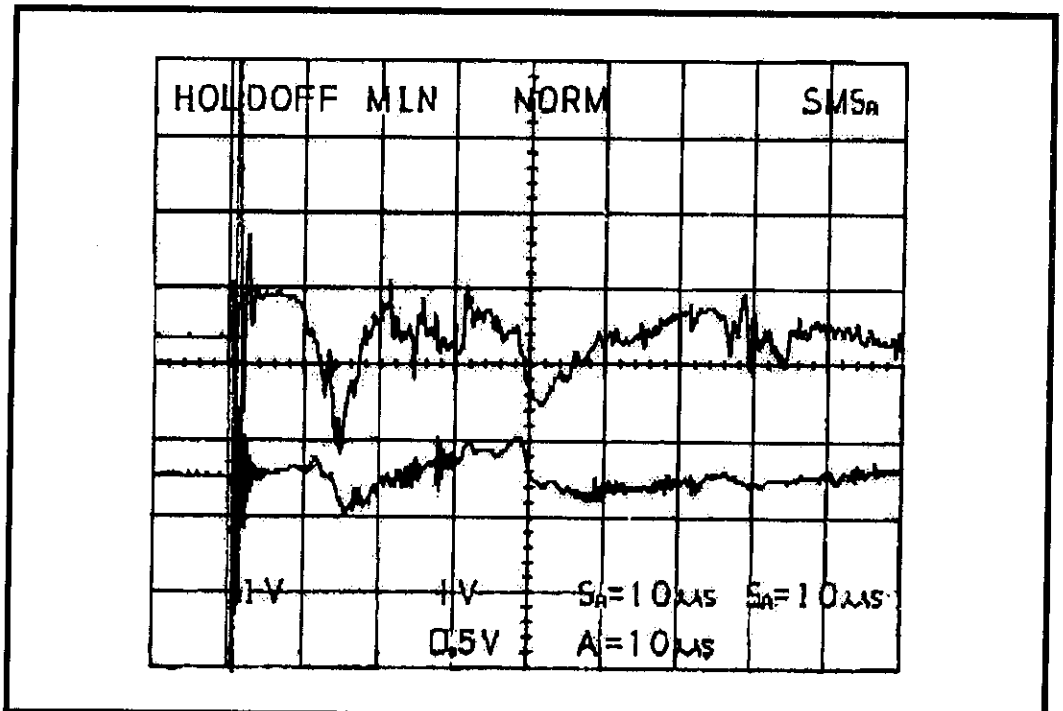


Fig. ( 4 – 26 ) Magnetic probes signals at 6 kV charging voltage, 1 Torr pressure and at a distance 1.7 cm above the inner electrode.

| Average position (cm) | Velocity at 1st peak ($10^6$ cm/s) | Velocity at 2nd peak ($10^6$ cm/s) |
|---|---|---|
| 0.7 | 4.667 | 5.600 |
| 1.7 | 3.500 | 3.111 |
| 2.7 | 1.333 | 1.217 |
| 3.7 | 2.800 | 1.867 |
| 4.7 | 7.000 | 3.733 |

Table ( 4 – 5 )

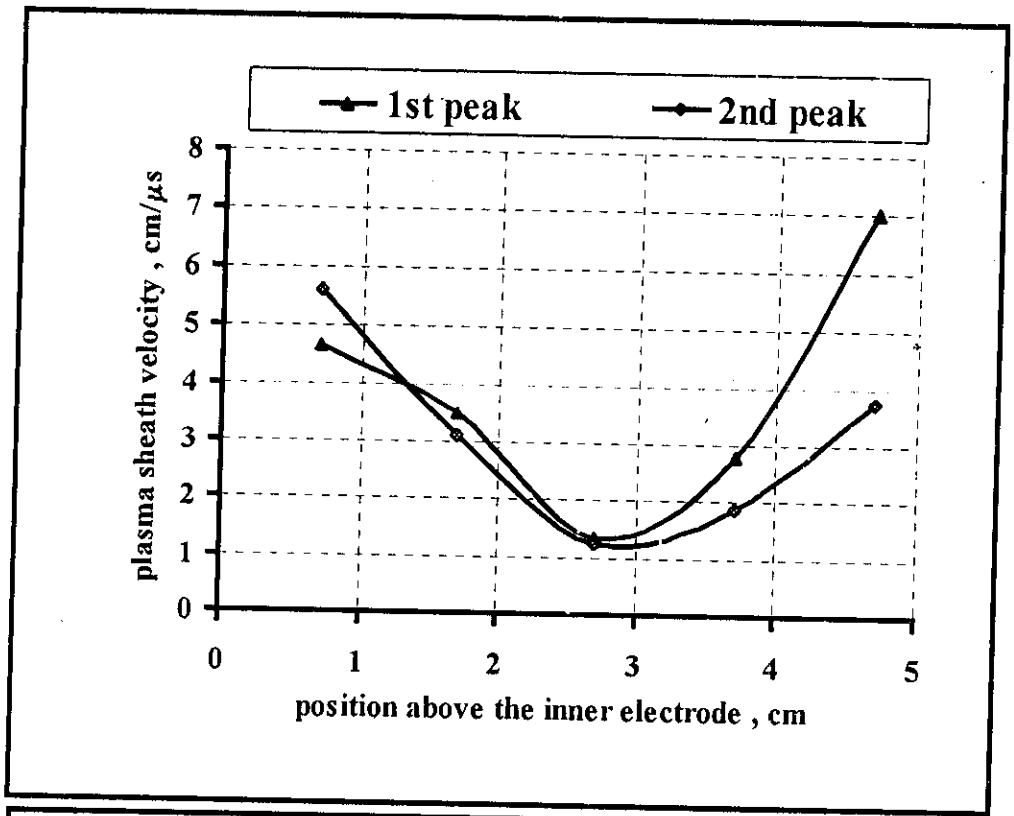


Fig. (4 – 27) Relation between the position above the inner electrode versus plasma sheath velocity at 3 kV charging voltage and 0.19 Torr pressure.

| Charging voltage (kV) | Velocity at 1st peak ($10^6$ cm/s) | Velocity at 2nd peak ($10^6$ cm/s) |
|---|---|---|
| 3 | 3.500 | 3.111 |
| 4.5 | 3.500 | 4.667 |
| 6 | 3.500 | 4.667 |

Table ( 4 – 6 )

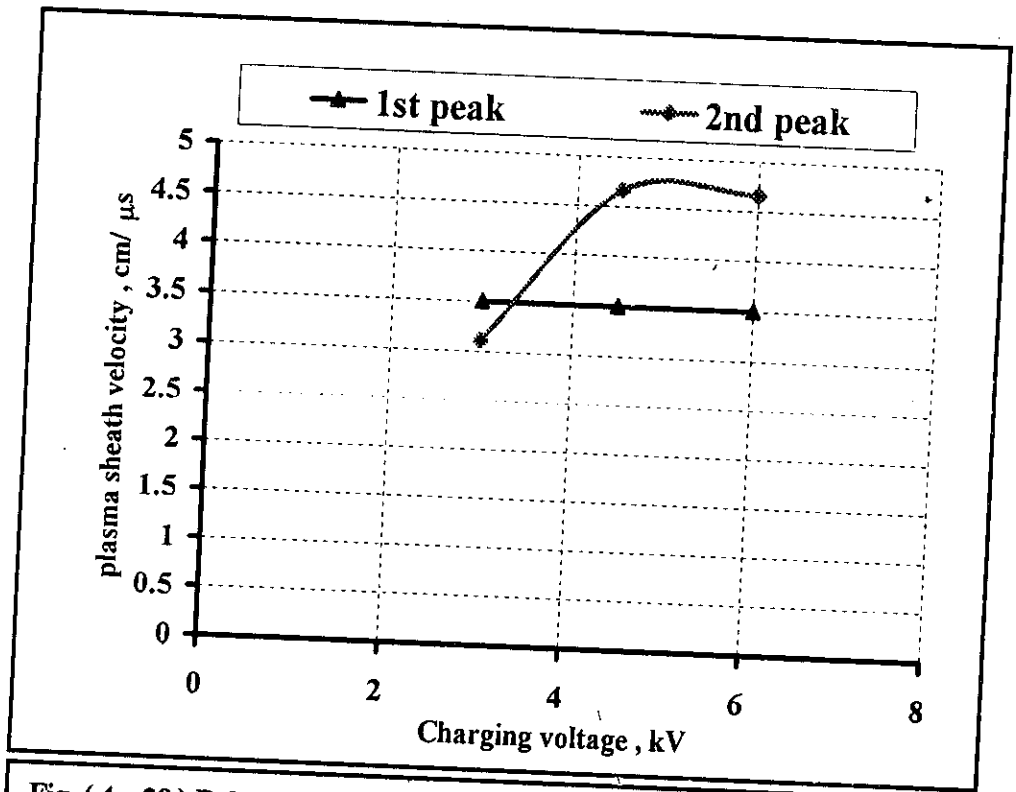


Fig. ( 4 – 28 ) Relation between the charging voltage versus plasma sheath velocity at 1.7 cm above the inner electrode and 0.19 Torr pressure.

## 4.6 ENERGY CALCULATIONS

The main task of this section is to calculate the system efficiency, which requires the calculation of the source energy, deposited energy and the summation of the kinetic and internal energies. All the calculations are made for 3 kV charging voltage and 0.19 Torr pressure.

### *4.6.1 Source Energy*

The source energy is calculated from the equation [6]

$$E_s = \tfrac{1}{2} CV^2 \qquad (4-14)$$

where $C$ is the total capacity of the condenser bank, and

$V$ is the charging voltage.

For *3 kV* charging voltage, *0.19 Torr* pressure and *46.26* $\mu F$ capacitance of the condenser bank, the source energy is equal to *208.17 Joule.*

### *4.6.2 Deposited Energy*

The deposited energy is that flow through the plasma source. This can be calculated from the power signal through the law

$$E_d = \int P\, dt \qquad (4-15)$$

The calculation shows that $E_u = 107.53$ *Joule.*

### *4.6.3 Kinetic Energy*

The kinetic energy can be calculated from the relation

$$K.E. = \tfrac{1}{2} m v_z^2 \qquad (4-16)$$

where

$m$ is the plasma sheath mass and

$v_z$ is the plasma sheath velocity due to the particle motion measured at the muzzle end.

The mass of the plasma sheath is given as

$m = \rho V$ where

$\rho$ is the average plasma density $= n_i \times$ *carbon atom mass* and

$V$ is the volume of the plasma sheath which is equal to

$V = \pi ( b^2 - a^2 ) l$, $l = v_z \times$ *plasma sheath time width*

where $b$ is the outer electrode radius = *4.2 cm*,

$a$ is the inner electrode radius = *2.6 cm* and

$l$ is the estimated plasma sheath length.

The kinetic energy is calculated for every half cycle with its variable changes such as the plasma velocity and density. The total kinetic energy is then equal to the summation of all kinetic energies for every half cycle.

$$K.E. = \Sigma \tfrac{1}{2} m v_z^2 \approx 10.976 \text{ Joule.}$$

### 4.6.4 *Internal Energy*

The internal energy is the energy exhausted to form the plasma, which can be calculated from the relation [6]

$$I.E. = n kT_e + n \varepsilon \qquad (4-17)$$

where

$n$ is the total number of the particles in the sheath.

$n = n_i \times V$ *( the volume of the plasma sheath )*

$kT_e$ is the plasma electron temperature.

$\varepsilon$ is the ionization energy ( = *1086 kJ/mole for carbon* ).

The internal energy is calculated with the same method used to calculate the kinetic energy so,

$$I.E. = \Sigma\, n\, kT_e + n\,\varepsilon \approx 0.156 + 0.590 = 0.746\ Joule.$$

### 4.6.5 Kinetic efficiency

The kinetic efficiency is the ratio between the kinetic energy and the deposited energy

$$kinetic\ effiency = \frac{kinetic\ energy}{deposited\ energy} \times 100 \quad \% \qquad (4-18)$$

Hence for *3 kV* charging voltage and *0.19 Torr* pressure one gets,

kinetic efficiency = *10.21* %

### 4.6.6 Internal efficiency

The internal efficiency is the ratio between the internal energy and the deposited energy

$$internal\ effiency = \frac{internal\ energy}{deposited\ energy} \times 100 \quad \% \qquad (4-19)$$

Hence for *3 kV* charging voltage and *0.19 Torr* pressure one gets,

internal efficiency = *0.69* %

### 4.6.7 Total efficiency

The total efficiency is the summation of the kinetic efficiency and the internal efficiency or it is the ratio between the summation of the kinetic energy and the internal energy to the deposited energy

$$total\ effiency = \frac{internal\ energy + kinetic\ energy}{deposited\ energy} \times 100\ \% \qquad (4-20)$$

Hence for *3 kV* charging voltage and *0.19 Torr* pressure one gets,

Total efficiency = *10.9* %

## 4.7 THEORETICAL ANALYSIS

In this section we will try to deduce the relation which can estimate the axial velocity $v_z$ and the position of the plasma sheath z with time $t$.

The summation of the forces act on the plasma sheath is equal to the rate of the momentum variation as in the following equation [26, 27]

$$\frac{d(mv)}{dt} = J \times B - \nabla P + \eta \nabla^2 v - mg \qquad (4-21)$$

Where, $J \times B$ is Lorentz force, ( *J is the current density and B is the magnetic field* ),

$\nabla P$ is the pressure gradient,

$\eta \nabla^2 v$ is the viscous force and $\eta$ is the coefficient of viscosity and

$mg$ is the gravitational force and $m$ is the mass of the ionized particles inside the sheath per unit volume and $g$ is the gravitational acceleration.

The sheath is propagated freely in evacuated medium, hence the given gradient pressure is neglected and approximately zero as well as viscous force, while the gravitational force is very small compared with Lorentz force, hence

$$m\frac{dv_z}{dt} = \vec{J} \times \vec{B} \qquad (4-22)$$

The current density $J$ and the magnetic field $B$ can be represented by $J=J_o \sin \omega t$, and $B=B_o \sin \omega t$ respectively, hence one get

$$m\int \frac{dv_z}{dt} = J_o B_o \sin^2 \omega t \qquad (4-23)$$

where $J_o$ is the peak current density and

$B_o$ is the peak magnetic field.

The axial velocity can be obtained by integrating the last equation and the substitute $sin^2 \omega t = \frac{1}{2}(1 - cos 2\omega t)$. hence

$$\int dv_z = \frac{J_o B_o}{2m} \int (1 - cos 2\omega t)\, dt$$

Then

$$v_z = \frac{J_o B_o}{2m}\left[ t - \frac{sin 2\omega t}{2\omega} \right] \qquad (4-24)$$

$$v_z = K\left[ t - \frac{sin 2\omega t}{2\omega} \right] \qquad (4-25)$$

The integration constant, $K$, can be determined from the initial conditions ( at $t = 0$ $v_z = 0$ ). Then $K$ is equal to

$$K = \frac{J_o B_o}{2m} \qquad (4-26)$$

By integrating equation ( 4 – 25 ), $z$ can be determined as follow,

$$v_z = \frac{dz}{dt} = K\left[ t - \frac{sin 2\omega t}{2\omega} \right] \qquad (4-27)$$

$$z = K \int \left[ t - \frac{sin 2\omega t}{2\omega} \right] dt$$

$$z = K\left\{ \left[ \frac{t^2}{2} + \frac{cos 2\omega t}{4\omega^2} \right] + C \right\} \qquad (4-28)$$

Hence the primary conditions is that $z = 0$ at $t = 0$, then the constant $C$ is calculated as

$$C = \frac{-1}{4\omega^2} \qquad (4-29)$$

Using $sin^2 \omega t = \frac{1}{2}(1 - cos 2\omega t)$, then $z$ is equal to

$$z = \frac{K}{2}\left[t^2 - \frac{sin^2 \omega t}{\omega^2}\right] \qquad (4-30)$$

From Ampere's law,

$$\int B.dl = \mu_o I$$

Then

$$2\pi r B_o = \mu_o I_o$$

Where

$I_o$ is the peak of the discharge current and $r$ is the radius at the point where the magnetic field is measured. For the first approximation, the mid point between the two electrodes is considered as $r$ = ½ ( $a + b$) where $a$, $b$ are the radius of the inner and outer electrodes respectively, hence

$$B_o = \frac{\mu_o I_o}{\pi(a+b)} \qquad (4-31)$$

for the current density $J_o$

$$J_o = \frac{I_o}{2\pi r \delta} = \frac{I_o}{\pi(a+b)\delta} \qquad (4-32)$$

Where, $\delta$ is the plasma sheath thickness.

Finally, for the mass per unit volume of the particles in the sheath $m'_v$, it is equal to the average plasma density so

$$m'_v = \rho \qquad (4-33)$$

Where

$\rho$ is the average plasma density $= n_i \times$ *carbon atom mass*

Substituting equations ( 4 – 31 ) , ( 4 – 32 ) and ( 4 – 33 ) into equation ( 4 – 26 ) one gets

$$K = \frac{\mu_o I^2_o}{2\pi^2 (a+b)^2 \delta \rho} \qquad (4-34)$$

Using the parameters of the present work, the constant $K$ according to ( 4 – 34 ) is equal to $2.37 \times 10^{14}$ ( $cm/sec^2$ ).

Table ( 4 – 7 ) shows the theoretical relation between the discharge time, the plasma sheath velocity and the position above the breaching end, also, Figs. ( 4 – 29 ) , ( 4 – 30 ) and ( 4 – 31 ) apply these relations graphically.

| Time ( μ s ) | Theoretical Position ( cm ) | Theoretical Velocity ($10^6$ cm/s) |
|---|---|---|
| 0.2 | 0.001 | 0.014 |
| 0.4 | 0.011 | 0.109 |
| 0.6 | 0.055 | 0.367 |
| 0.8 | 0.174 | 0.869 |
| 1 | 0.424 | 1.696 |
| 1.2 | 0.879 | 2.928 |
| 1.4 | 1.628 | 4.644 |
| 1.6 | 2.774 | 6.923 |
| 1.8 | 4.440 | 9.843 |
| 2 | 6.760 | 13.481 |
| 2.2 | 9.885 | 17.910 |
| 2.4 | 13.982 | 23.207 |
| 2.6 | 19.230 | 29.442 |
| 2.8 | 25.826 | 36.687 |
| 3 | 33.977 | 45.010 |

Table ( 4 – 7 )

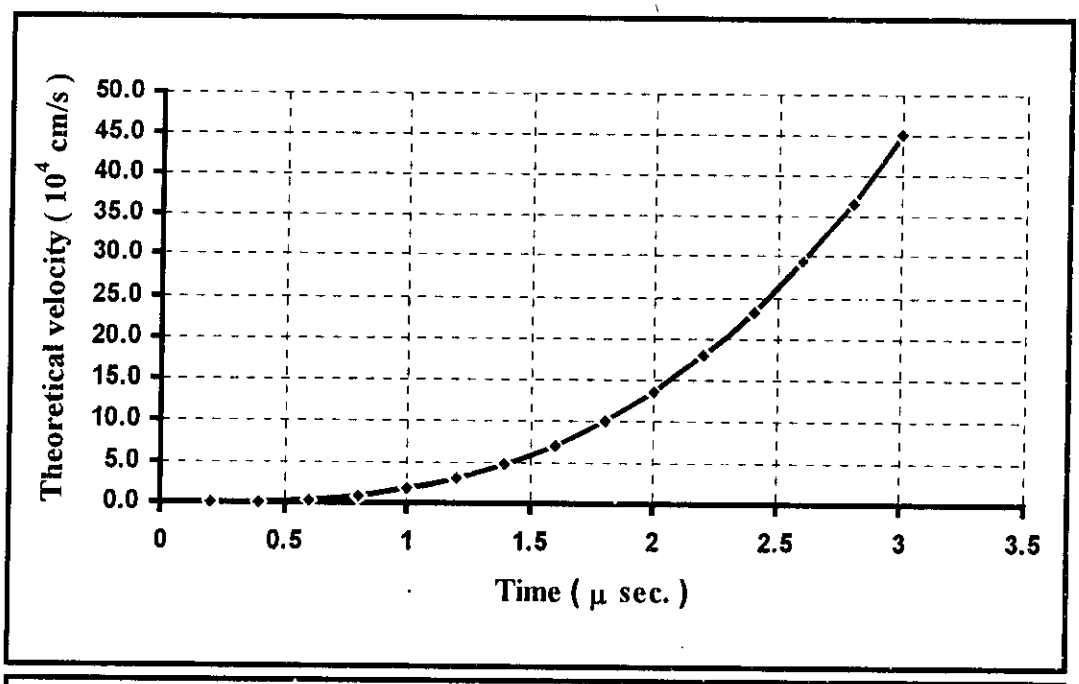


Fig. ( 4 – 29 ) Theoretical relation between the velocity versus the discharge time at 3 kV charging voltage and 0.19 Torr pressure.

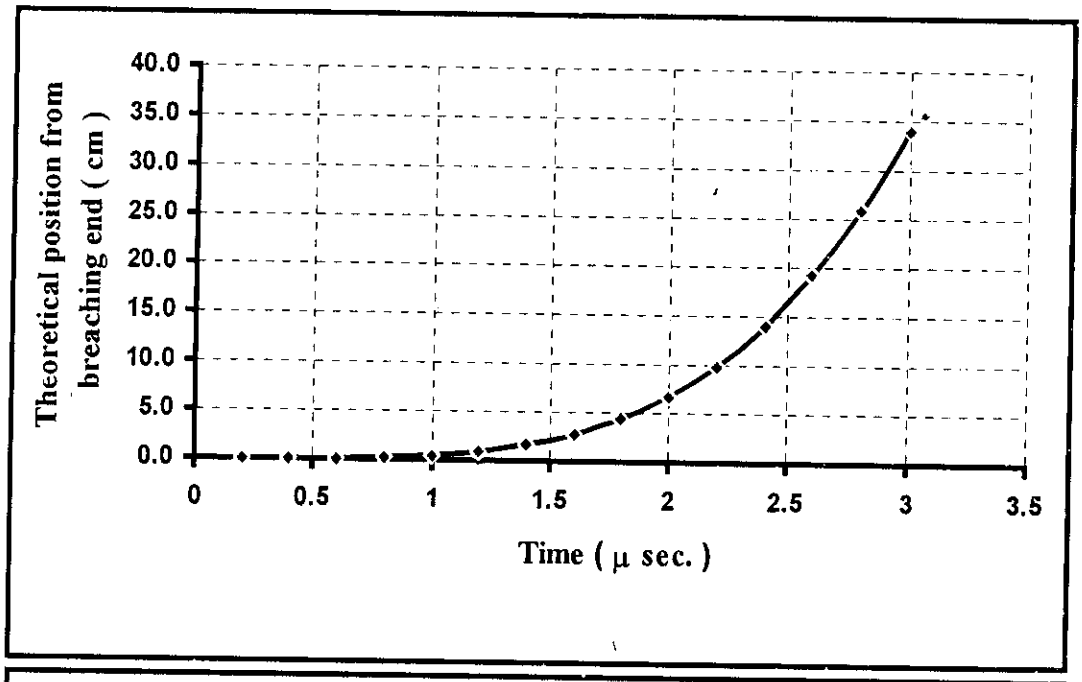


Fig. (4–30) Theoretical relation between position from the breach versus the discharge time at 3 kV charging voltage and 0.19 Torr pressure.

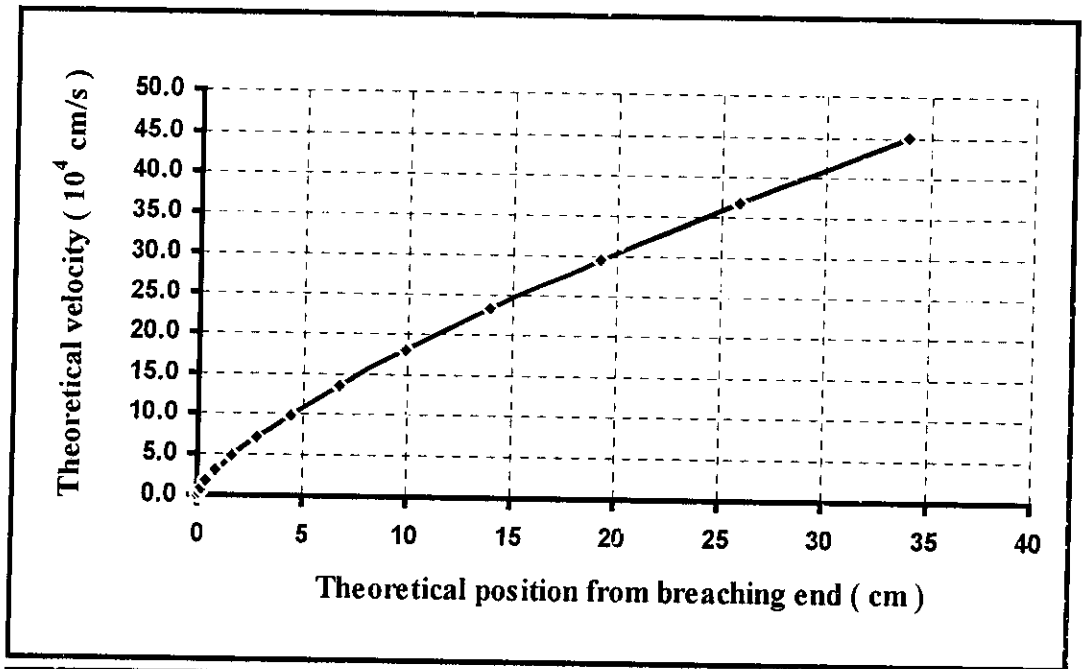


Fig. (4 – 31) Theoretical relation between the velocity versus the position from the breach at 3 kV charging voltage and 0.19 Torr pressure.

# CHAPTER V

# DEPOSITED THIN FILM ANALYSIS

## 5.1 INTRODUCTION

The aim of this chapter is to study the plasma deposited material variation with the different discharge parameters studied in the previous chapters. In this chapter the deposited material on glass substrate from ceramic and graphite powders are analyzed, where these powders are placed at the breach of the plasma coaxial accelerator system. The analysis of these substrates are done by more than one method. First, some substrates are magnified and photographed using scanning electron microscope ( *SEM* ). In the second method, the substrates are scanned by microdensitometer device to get the deposited material thickness relative to a reference with well known thickness. In the last method, an experiment of interference by reflection using laser device takes place in order to determine the accurate thin film thickness of the powder deposited on the reference substrate.

## 5.2 SEM ANALYSIS

The first method in the study of the material deposited on the glass substrate is made using scanning electron microscope analysis ( *SEM* ). Figures ( 5 – 1 ), ( 5 - 2 ) and ( 5 - 3 ) show the grains of the ceramic powder deposited on the glass substrates enlarged *1400* times and Figs. from ( 5 - 4 ) to ( 5 - 7 ) show the grains of the graphite powder deposited on the glass substrates enlarged *700* times.

The main remark on these figures is the existence of some clusters. Also, for the graphite figures , the main remark which does not appear, due to their black and white color degrees, is that there is some clusters shows a light spectrum ( *dispersion* ) which may be due to the formation of diamond crystals or DLC film.

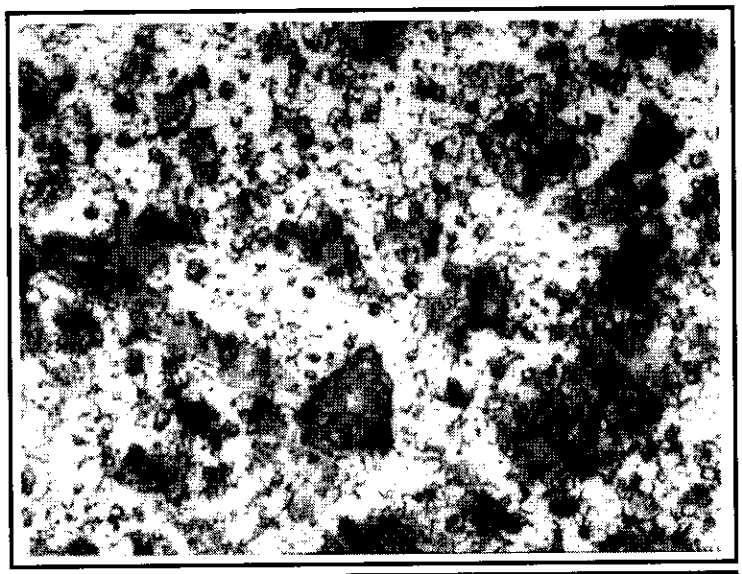

Fig. ( 5 – 1 ) SEM micrograph of surface morphology of ceramic film on glass substrate at 6 kV and 100 pulses.

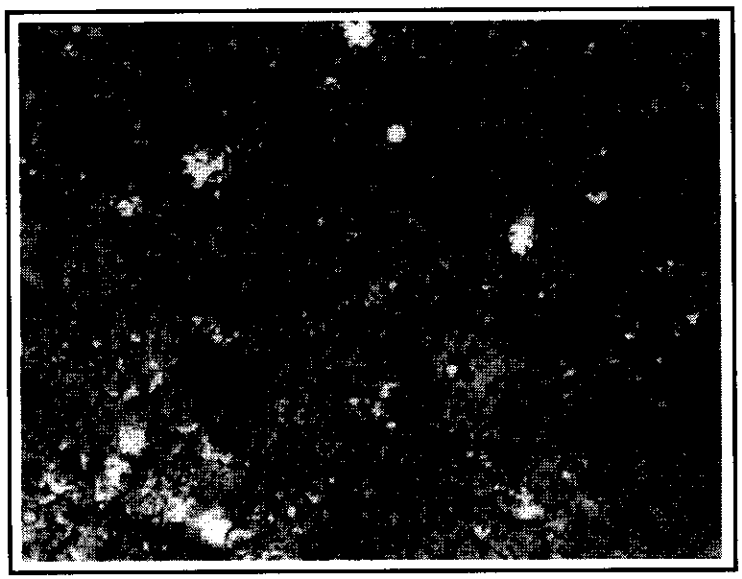

Fig. ( 5 – 2 ) SEM micrograph of surface morphology of ceramic film on glass substrate at 5.5 kV and 100 pulses.

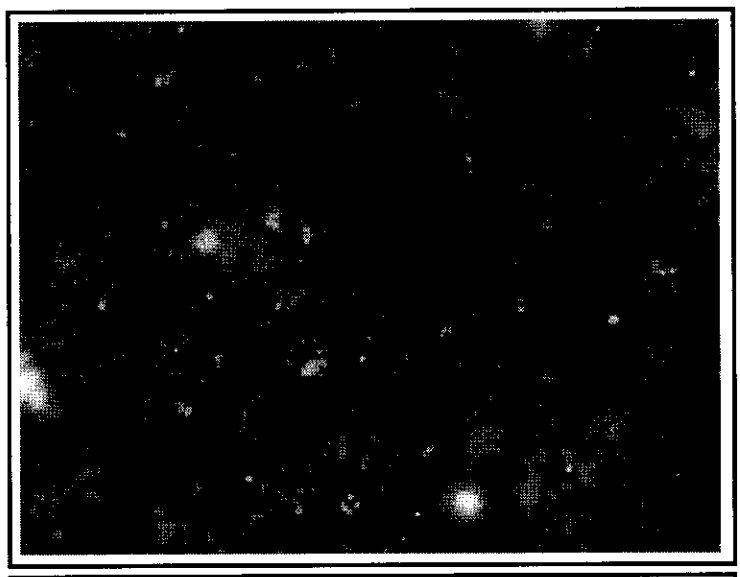

Fig. ( 5 – 3 ) SEM micrograph of surface morphology of ceramic film on glass substrate at 6 kV and 100 pulses.

Fig. ( 5 – 4 ) SEM micrograph of surface morphology of graphite film on glass substrate at 5.9 kV and 25 pulses.

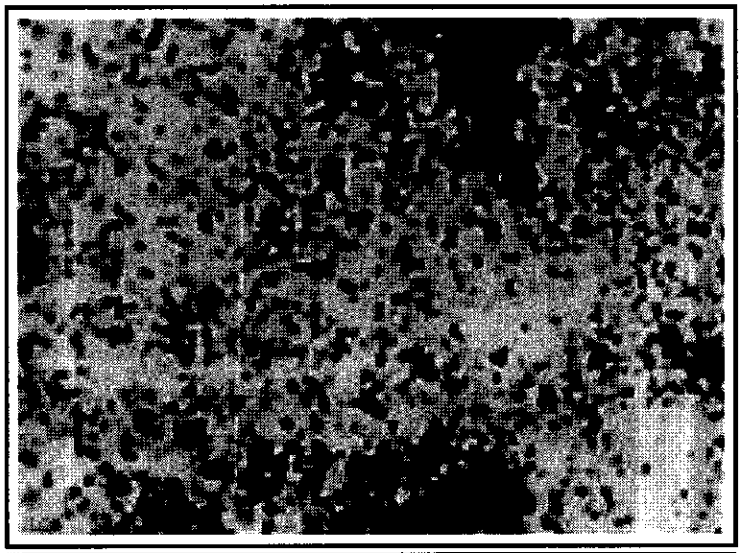

Fig. ( 5 – 5 ) SEM micrograph of surface morphology of graphite film on glass substrate at 8 kV and 50 pulses.

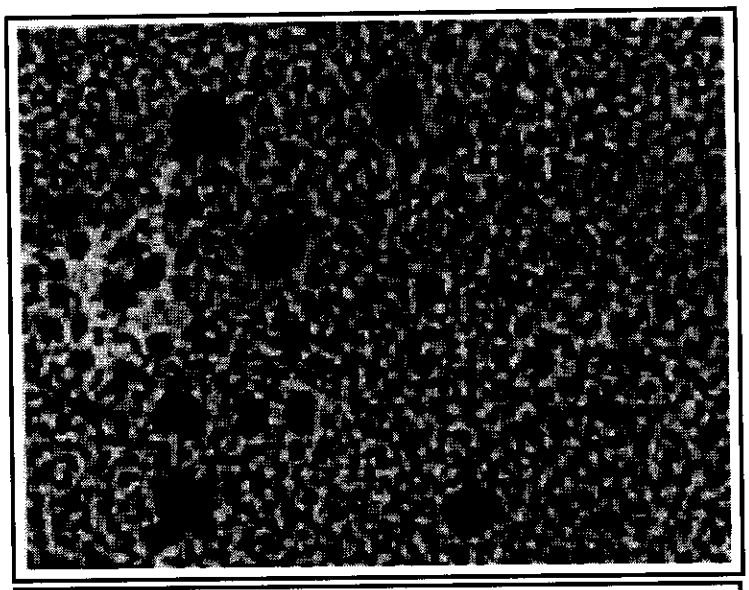

Fig. ( 5 – 6 ) SEM micrograph of surface morphology of graphite film on glass substrate at 10.5 kV and 100 pulses.

Fig. ( 5 – 7 ) SEM micrograph of surface morphology of graphite film on glass substrate at 11.5 kV and 25 pulses.

A study of the grains distribution according to its diameter for ceramic film on the glass substrate at *6 kV* charging voltage and *100 pulses* ( *conditions of Fig.* ( 5 - 1 )) is shown in Fig. ( 5 – 8 ) . In this figure it is clear that the grains seems similar to Maxwellian distribution approximately.

Figure ( 5 – 8 ) shows also that the grains have a diameters of a range between about *0.15* μ*m* to *3.6* μ*m* , while the peak grain density was at grain diameter of *0.54* μ*m.*

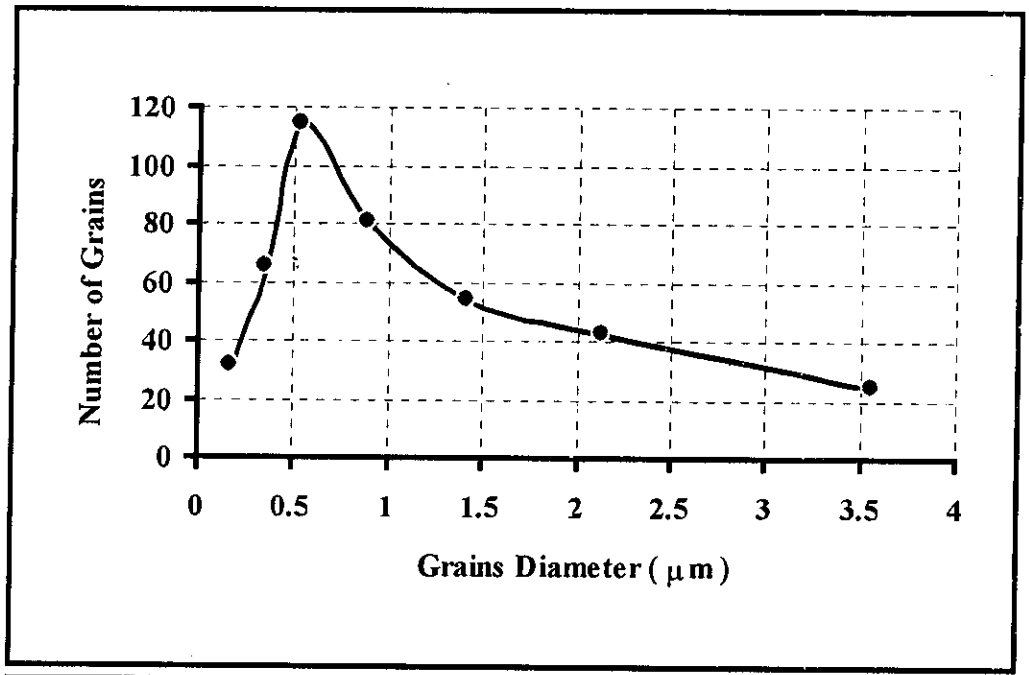


Fig. ( 5 – 8 ) Grains distribution according to its diameter for ceramic film on glass substrate at 6 kV and 100 pulses.

## 5.3 DEPOSITED MATERIAL THICKNESS

The aim of the present sections is to explain the methods, which used in order to estimate the thickness of the thin film of the graphite powder deposited on the glass substrates. This can help us to obtain the relation between the thin film thickness variation with both the charging energy and the number of pulses.

### *5.3.1 Interferometery for Thickness Measurements*

Figure ( 5 – 9 ) shows the experimental arrangement used to measure accurately the absolute thickness of the graphite thin film.

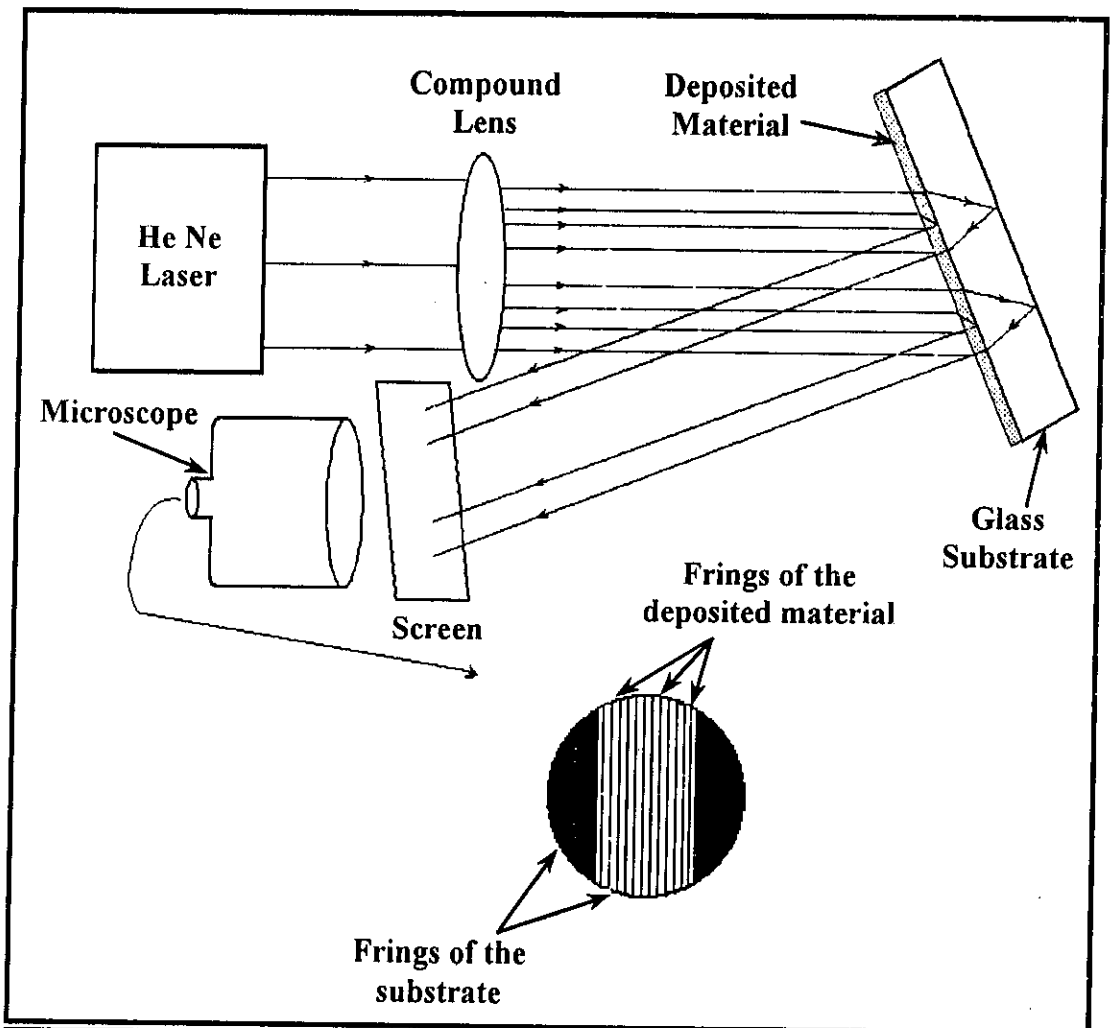


Fig. ( 5 – 9 ) Laser interferometer with microscope arrangement.

As shown in the last figure, the system used to determine the thin film thickness depends on the interference phenomena and it consists of the following components :

1. *He Ne Laser Source; which used to emit the laser beam.*
2. *Compound Lens; to enlarge the laser beam.*
3. *The Glass Substrate; which is the material to be measured.*
4. *Receiver Screen; to receive the interference frings.*
5. *Microscope; to enlarge the image obtained on the receiver screen.*

The main idea in this system measurements is as follows: when the interference frings appears one can see the wide frings ( *which can be seen by the eye* ). Each fring contains number of thin frings inside itself (*which can be seen easly by the microscope*). The wide frings appear due to the interference of the glass substrate sides itself and the thin frings appear due to the interference from the sides of the deposited graphite itself.

Consider $d$ is the glass substrate thickness, $t$ is the deposited graphite thickness, $\delta$ is the width of frings of the substrate and $\sigma$ is the graphite frings width, one gets

$$\frac{d}{\delta} = \frac{t}{\sigma} \qquad (5-1)$$

Where we have omit the refractive indices of the graphite and the glass substrate since they are close together.

In the present work and for the chosen reference glass substrate, $\delta = 300\ \sigma$ and $d = 1$ mm then, as substituted in equation ( 5 - 1 ), one can get, $t \approx 3.333\ \mu m$.

This thickness is for graphite with charging voltage of *8 kV* and with *50 discharge pulses.*

### 5.3.2 *Microdensitometer for Relative Thickness Measurement*

The aim of this measurement is to obtain the thickness of the deposited graphite of all glass substrates; this is made by measuring the relative thickness of all substrates as compared to the known substrate thickness, which is measured accurately in the previous section. The device used in these measurements is the microdensitometer of type *MK III C made by JOYCE and LOEBL, England.*

The microdensitometer device is used to obtain charts like that shown in Fig. ( 5 – 10 ). At the first sight on these charts, one can get the variation of the thickness of the deposited material on the glass substrate. The second step is to measure the average height of the chart peaks for every slice and divide them by the height of the chart of the reference substrate to obtain the relative thickness.

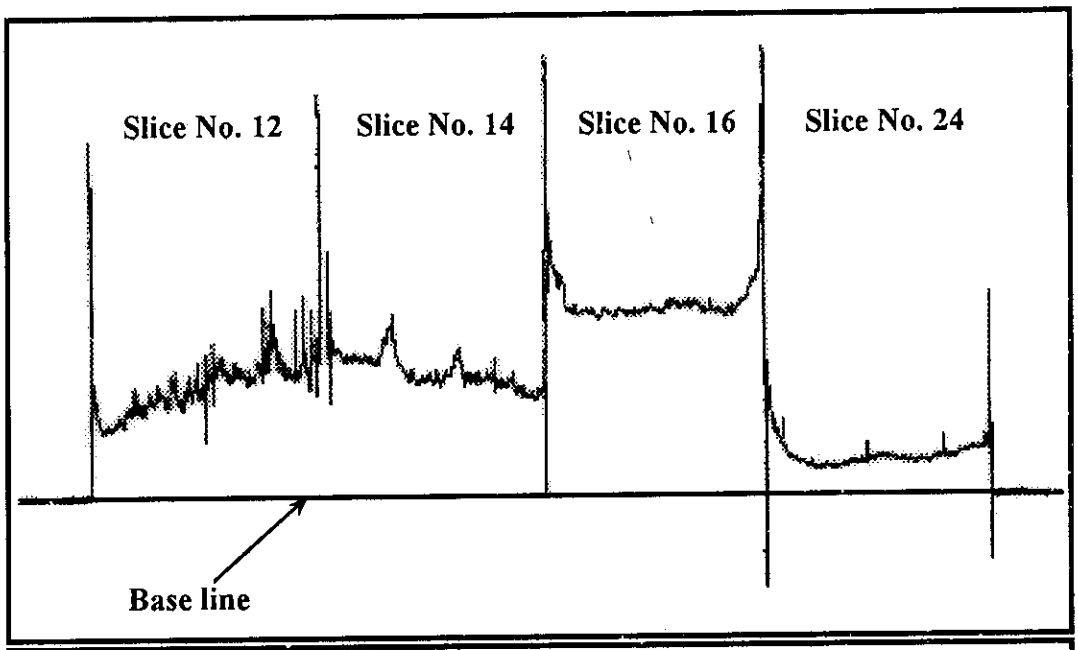


Fig. ( 5 – 10 ) Microdensitometer chart to obtain the relative thickness.

As an application of these measurements, the charts of *13* glass substrates for the graphite deposited material are obtained at various conditions of the charging voltage and number of pulses. Figure ( 5 – 11 ) shows the relation between the thickness of the deposited material with number of pulses at *5.9 kV* charging voltage which illustrated in Table ( 5 - 1 ). Figure ( 5 – 12 ) shows the relation between the thickness per pulse of the deposited material and charging energy for 25 and 50 pulses which illustrated in table ( 5 - 2 ).

As shown in Fig. ( 5 - 11 ) the deposited material thickness is directly related to the number of pulses with linear increment relation. Also Fig. ( 5 - 12 ) shows that the thickness per pulse for the deposited material seems to increase exponentially with increasing the charging energy.

To calculate the thickness of the substrates, consider $t$ is thickness of the deposited material on the reference substrate which illustrated in equation ( 5 – 1 ) and $\alpha$ is the relative thickness of the deposited material in the wanted substrate which equals the average height of the chart of that substrate as that in Fig. ( 5 - 10 ) divided by that of the reference substrate and $\zeta$ is the thickness to be measured. Then one can write

$$\zeta = t \times \alpha \qquad (5-2)$$

and for our experiment $t \approx 3.333\ \mu m$ then one gets

$$\zeta\ (\mu m) = 3.333 \times \alpha \qquad (5-3)$$

| Number of shots | Average chart height ( cm ) | Relative density | Absolute thickness ( μm ) |
|---|---|---|---|
| 5 | 0.05 | 0.024 | 0.079 |
| 10 | 0.1 | 0.048 | 0.159 |
| 15 | 0.15 | 0.071 | 0.238 |
| 20 | 0.2 | 0.095 | 0.317 |
| 25 | 0.25 | 0.119 | 0.397 |
| 50 | 0.55 | 0.262 | 0.873 |
| 75 | 1.15 | 0.460 | 1.533 |

Table ( 5 - 1 )

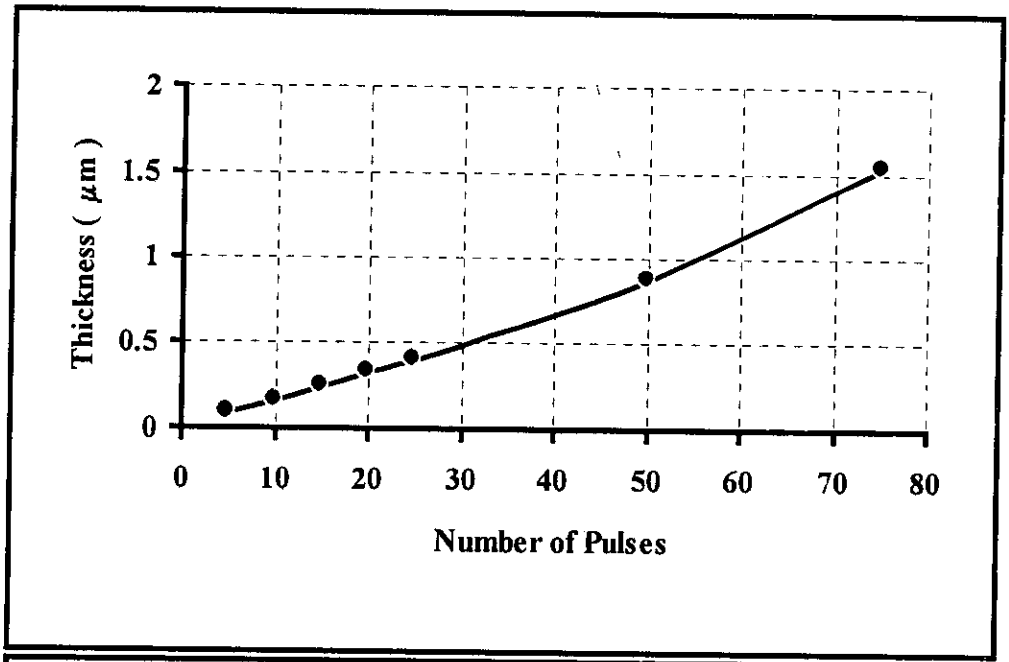


Fig. ( 5 – 11 ) Relation between the deposited material thickness with number of pulses at 5.9 kV charging voltage.

| No of shots | Charging voltage ( kV ) | Charging energy ( kJ ) | Average chart height ( cm ) | Rel. thick. | Abs. Thick. ( μm ) | Thickness per pulse |
|---|---|---|---|---|---|---|
| 25 | 5.9 | 0.805 | 0.25 | 0.119 | 0.397 | 0.016 |
| 25 | 8.5 | 1.671 | 0.65 | 0.310 | 1.032 | 0.041 |
| 25 | 11 | 2.799 | 3.1 | 1.192 | 3.974 | 0.159 |
| 25 | 11.5 | 3.059 | 4.2 | 1.615 | 5.384 | 0.215 |
| 50 | 5.9 | 0.805 | 0.55 | 0.262 | 0.873 | 0.017 |
| 50 | 8 | 1.480 | 2.1 | 1.000 | 3.333 | 0.067 |
| 50 | 8.2 | 1.555 | 2.8 | 0.966 | 3.218 | 0.064 |
| 50 | 11.2 | 2.901 | 7.85 | 3.738 | 12.459 | 0.249 |

Table ( 5 - 2 )

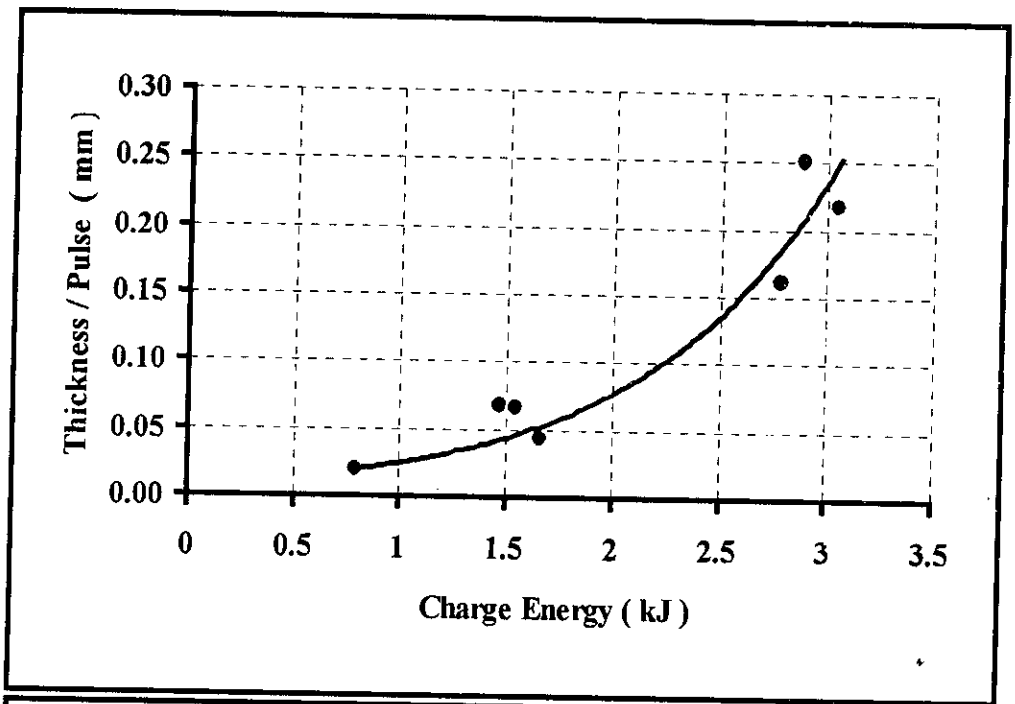


Fig. ( 5 – 12 ) Relation between the deposited material thickness per pulse with charging energy.

## 5.4 CONCLUSION

The deposition process is studied in the present work as one of the plasma processes applications. For this study, the scanning electron microscope ( *SEM* ) analysis and suitable arrangement of laser interferometer and microscope were used.

The study of the ceramic and graphite powders using SEM analysis showed the formation of a homogeneous distribution of the deposited material. It is seen that the grains follow certain distribution according to its size distribution where the grains diameters were of a range between *0.15* $\mu m$ and *3.6* $\mu m$ and the peak grain density was at grain diameter of *0.54* $\mu m$. It is also seen that for the graphite, a diamond crystals or DLC films may be formed with small ratio but not confirmed.

The study of the deposited material thickness using the laser interferometer arrangement shows a linear relation dependence of the deposited material thickness with number of pulses and the deposited thickness increased exponentially with capacitor bank charging energy.